國立臺灣大學醫學院基因體暨蛋白體醫學研究所

博士論文

Graduate Institute of Medical Genomics and Proteomics

College of Medicine

National Taiwan University

Doctoral Dissertation

RRBP1透過調控腎素之胞內運輸調節血壓及鉀離子恆定

RRBP1 regulates blood pressure and potassium homeostasis by

modulating intracellular renin trafficking

邱楚璿

Chu-Hsuan Chiu

指導教授：張以承 博士

Advisor: Yi-Cheng Chang M.D. Ph.D.

中華民國 112 年 5 月

May 2023

國立臺灣大學博士學位論文

口試委員會審定書

PhD DISSERTATION ACCEPTANCE CERTIFICATE
NATIONAL TAIWAN UNIVERSITY

RRBP1 透過調控腎素之胞內運輸調節血壓及鉀離子恆定

RRBP1 regulates blood pressure and potassium homeostasis by modulating intracellular renin trafficking

本論文係__邱楚璿__(姓名)_D05455001_（學號）在國立臺灣大學___基因體暨蛋白體醫學研究所__(系/所/學位學程)完成之博士學位論文，於民國_112_年_05_月_31_日承下列考試委員審查通過及口試及格，特此證明。

The undersigned, appointed by the ___Graduate Institute of Medical Genomics and Proteomics___
on ___31___ (date)__May__ (month)___2023___ (year) have examined a PhD dissertation entitled above presented by Chu-Hsuan Chiu (name) D05455001 (student ID) candidate and hereby certify that it is worthy of acceptance.

口試委員 Oral examination committee:

（指導教授 Advisor）

系主任/所長 Director:

誌謝

本論文的完成離不開許多人的支持和幫助，在此向他們表示衷心的感謝。

首先，我要感謝我的指導教授 張以承 醫師，您的耐心指導和適時地讓我主導我論文的研究方向讓我更深入地理解研究領域的複雜性，並且在解決困難和面對挑戰時給予了我寶貴的支持。另外，也感謝老師在我博士班期間給予我額外經濟上的支持，讓我更加無後顧之憂地投入研究工作。我還要感謝我所有的口試委員，包括林石化教授、吳允升教授、潘思樺老師、莊立民醫師這幾年來給我寶貴的建議，以及實質上的實驗合作，讓我更加進步，也幫助我的研究一步一步的完成，尤其感謝莊立民教授，身為我的 mentor 每個月兩次的 lab meeting，給予我很多的協助與建議，對我來說非常珍貴。

此外，我要感謝實驗室所有的同事和其他研究生包括璧瑜學姊、君怡、孟倫、曉苓學姊、曉薇學姊、曉玫學姊、為舜學姊、國璨…等等（族繁不及備載）對於我研究上的建議與實驗上的幫忙。感謝你們在研究過程中的合作和討論，我從你們的經驗和洞察力中受益匪淺。我也要特別感謝陳寬幫我繪製了精美的摘要結論圖，讓我順利地發表 paper。在你們的幫助下，我得以克服許多困難，並取得了令人滿意的結果。

同樣地，我要感謝我的媽媽、兩個姊姊和朋友。感謝你們無私的支持和鼓勵，你們的愛和關心是我前進的動力。感謝你們在我需要的時候總是站在我身邊，給予我精神上的支持和鼓勵。

摘要

RRBP1，又被稱為 p180，是一種與內質網核糖體結合的蛋白。許多全基因組關聯分析的研究指出，RRBP1 基因的變異與動脈硬化心血管疾病以及血液中的血脂蛋白含量有高度相關性。然而，關於 RRBP1 在調控心血管疾病中最重要的因素之一——「血壓」的角色，目前尚未被廣泛探討。本研究的主要目的在於釐清 RRBP1 在調控血壓以及在心血管生理上所扮演的角色。

首先，我們利用史丹佛亞洲及太平洋高血壓及胰島素阻抗計畫（Stanford Asia-Pacific Program for Hypertension and Insulin Resistance）中的世代研究資料庫，透過全基因組連鎖分析，發現 RRBP1 的基因變異與血壓有高度相關性。此外，我們進一步進行了 Rrbp1 基因剔除小鼠的實驗，結果顯示這些小鼠表現出低血壓並出現早發型未預期的猝死。透過血液生化檢測，我們發現 Rrbp1 基因剔除小鼠患有低腎素型低醛固酮血症（hyporeninemic hypoaldosteronism），且伴隨高血鉀（hyperkalemia）症候群。在高鉀離子飲食攝入的壓力下，Rrbp1 基因剔除小鼠表現出嚴重的高血鉀誘發心律不整（arrhythmia），並顯著增加死亡率。然而，透過氟氫可體松（Fludrocortisone）的治療，可以有效降低 Rrbp1 基因剔除小鼠在高鉀離子飲食攝入後的血鉀濃度以及死亡率。

此外，利用免疫組織化學染色法標定腎臟切片中腎素發現在 Rrbp1 基因剔除小鼠之腎臟組織切片的腎素含量明顯高於野生型小鼠。相似的是，我們利用免疫金染色標定 RRBP1 基因敲弱（RRBP1-kcockdown）的人類腎素生產細胞株（Calu-6）之腎素發現 RRBP1 基因敲弱後，腎素大量累積在細胞內。同時，免疫螢光染色發現 RRBP1 基因敲弱後，影響了腎素從內質網運輸到高基氏體的效率。本研究發現

RRBP1 藉由影響腎素在細胞內的運輸調控生理血壓以及血鉀扮演重要的角色。

關鍵字: RRBP1、血壓、腎素、高血鉀、心律不整、猝死

Abstract

RRBP1, also known as ER ribosomal-binding protein 1 or p180, has been implicated in various cardiovascular diseases through genetic variants identified in numerous genome-wide association studies. However, the precise role of RRBP1 in the regulation of blood pressure remains undefined. In this study, we aimed to elucidate the impact of RRBP1 on blood pressure regulation and its role in cardiovascular physiology.

In the Stanford Asia-Pacific Program for Hypertension and Insulin Resistance (SAPPHIRe) cohort, our research team conducted a genome-wide linkage analysis followed by regional fine mapping. This comprehensive approach enabled us to identify noteworthy genetic variants within the RRBP1 gene, demonstrating a significant association with blood pressure. To investigate the functional implications of RRBP1, we generated a transgenic mouse model. *Rrbp1*-knockout mice exhibited lower blood pressure and increased susceptibility to sudden cardiac death, which was attributed to hyporeninemic hypoaldosteronism-induced hyperkalemia. Significantly, when subjected to high potassium intake, Rrbp1-knockout mice exhibited a noteworthy decrease in survival rate compared to their wild-type counterparts. Remarkably, these Rrbp1-knockout mice displayed severe lethal arrhythmia induced by hyperkalemia and persistent hypoaldosteronism, particularly under conditions of elevated potassium intake. However, treatment with fludrocortisone effectively rescued these phenotypes.

Immunohistochemistry analysis revealed the accumulation of renin within the kidneys of *Rrbp1*-knockout mice, indicating impaired renin-angiotensin-aldosterone system (RAAS) function. Furthermore, our investigations confirmed that renin predominantly accumulated within the endoplasmic reticulum (ER) and exhibited compromised transport to the Golgi apparatus in RRBP1-knockdown (-KD) Calu-6 cells. This impaired secretion of renin was substantiated through detailed examinations using transmission
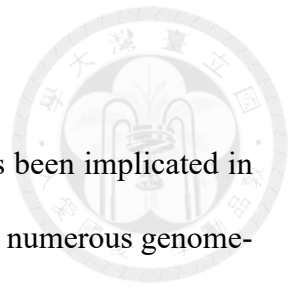
electron and confocal microscopy. In parallel, our human genetic studies revealed a significant association between RRBP1 genetic variants and blood pressure. Notably, consistent with the findings in our mouse model, mice lacking RRBP1 exhibited lower levels of plasma renin and aldosterone, resulting in reduced blood pressure, severe hyperkalemia, and cardiac sudden death.

Collectively, our study provides novel insights into the role of RRBP1 as a modulator of the renin-angiotensin-aldosterone system (RAAS), affecting blood pressure regulation and potassium homeostasis.
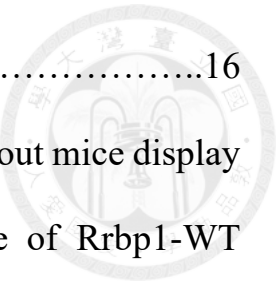
Key words: Arrhythmia, blood pressure, hyperkalemia, renin, RRBP1, sudden death
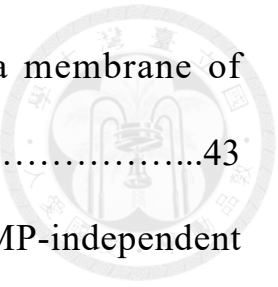
Table of contents

List of figures

List of tables

1. Introduction

1-1 Cardiovascular diseases

According to the World Health Organization (WHO), cardiovascular diseases (CVDs) are the leading cause of death worldwide. CVDs encompass a range of heart and blood vessel disorders and are responsible for approximately 17.9 million deaths annually. Among these diseases, atherosclerotic cardiovascular disease, which includes conditions such as ischemic heart disease, stroke, hypertensive heart disease, aortic aneurysm, and peripheral arterial diseases, remains a significant global health burden [1]. Traditional risk factors for CVDs include dyslipidemia, high blood pressure, tobacco smoking, and type 2 diabetes [1]. To further our understanding of the genetic basis of CVDs and related conditions, several large-scale genome-wide association studies (GWAS) have been conducted [2-10].

1-2 Hypertension

Hypertension, characterized by elevated blood pressure with a systolic blood pressure of 140mmHg or higher and/or a diastolic blood pressure of 90mmHg or higher, is a common symptom and a significant risk factor for cardiovascular diseases (CVDs), premature death, and disability worldwide [11-13]. The prevalence of hypertension is increasing due to various modern lifestyle risk factors, including unhealthy diets high in fat and salt, an aging population, insufficient physical activity, and genetic factors [12, 14]. According to the World Health Organization (WHO), there are currently 1.13 billion people living with hypertension, with a disproportionate burden on low- and middle-income countries [14]. Addressing hypertension and its associated risk factors is crucial for preventing CVDs and reducing the global burden of disease.

1-3　Renin-angiotensin-aldosterone system

The renin-angiotensin-aldosterone system (RAAS) is a crucial hormone system involving multiple organs in the body, responsible for regulating blood pressure, electrolyte balance, and cardiovascular and renal function [15-17]. It consists of three main components: renin, angiotensin, and aldosterone. Renin is primarily secreted into the bloodstream by juxtaglomerular (JG) cells located within the renal juxtaglomerular apparatus in the kidney [18, 19]. Once released, renin acts on angiotensinogen, a protein produced continuously by the liver. Angiotensinogen, a member of the non-inhibitory serine protease inhibitor superfamily, consists of 485 amino acids and exists in both a basic form with a molecular weight of 53 kDa and a glycosylated form with a weight of 75 kDa [20, 21]. The cleavage of angiotensinogen by renin is the rate-limiting step in the activation of the RAAS. It is important to note that renin exhibits species specificity, with human renin cleaving human angiotensinogen but not mouse angiotensinogen [22, 23].

The cleavage of ten amino acids from the N-terminal of angiotensinogen by renin leads to the formation of angiotensin I, a decapeptide. Angiotensin I is further converted into angiotensin II, an octapeptide, by the action of angiotensin-converting enzyme (ACE) [24-26]. ACE is predominantly found in vascular endothelial cells within lung tissue. The cleavage of angiotensin I by ACE is crucial for its activation, as angiotensin I is relatively inactive or less active on angiotensin receptors [27, 28]. Angiotensin II, composed of eight amino acids (Asp-Arg-Val-Tyr-Ile-His-Pro-Phe), plays a critical role in both physiological and pathophysiological processes. It exhibits positive inotropic and chronotropic effects, promotes vasoconstriction, and enhances salt intake [29-32]. The receptors for angiotensin II, AGTR1 and AGTR2, belong to

the superfamily of seven-transmembrane G protein-coupled receptors [33]. Activation of the AGTR pathway by angiotensin II stimulates aldosterone production.

Aldosterone, a steroid hormone, is primarily synthesized in the zona glomerulosa of the adrenal cortex. As a mineralocorticoid, aldosterone regulates electrolyte and fluid homeostasis [34-37]. The aldosterone-mineralocorticoid receptor complex acts as a transcription factor, inducing the expression of serum and glucocorticoid-inducible kinase 1 (Sgk1), corticosteroid hormone-induced factor (CHIF), and Kirsten Ras (Ki-ras) [38]. This, in turn, leads to increased expression and activity of the luminal amiloride-sensitive epithelial Na+ channel (ENaC), responsible for sodium reabsorption, and the renal outer medullary potassium channel (ROMK), which facilitates potassium secretion [39, 40].

1-4   Renin

Renin is the key hormone which controls the rate limiting step of RAAS regulates blood pressure, physiological functions, and various pathophysiological disorders [41]. Renin, an aspartyl-protease, initiates the cascade of RAAS by cleavage of angiotensinogen into angiotensin-I exclusively [42]. The basic physiological functions of renin are regulation of blood pressure, electrolytes and volume homeostasis, cell growth, and even apoptosis [43]. Local RAAS in various tissue has quite different mode of actions [44]. Other tissues also express and secrete renin which exhibit distinct biological roles. The signal peptides of renin which is encoded by exon 1 is required secretory pathway and transportation to ER of renin. Cytosolic renin which is encoded by exon 1A-9 exhibits non-secretory pathway [45]. In adrenal gland, there are both secretory and cytosolic renin which is found in mitochondria.
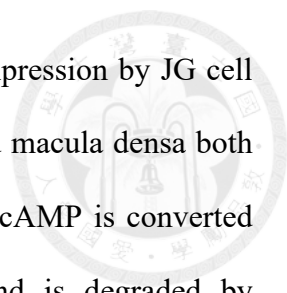
Cytosolic renin in mitochondria increases aldosterone production in a secretory renin-independent way [46, 47]. Cytosolic renin is also associated with hypertrophy and overexpression under myocardial infarction [45, 48].

Various tissues produce renin but only juxtaglomerular (JG) cells in kidney produce active form of renin. There are multiple regions in renin gene are identified to regulate activation or suppression of renin gene transcription [41, 49]. Cyclic adenosine monophosphate (cAMP)- responsive element binding protein (CREB) and peroxisome proliferator-activated receptor-γ (PPAR-γ) confer a positive effect on renin gene expression [50, 51]. On the contrary, vitamin-D3 and transcription nuclear factor-κB (NF-κB) inhibit the CREB-induced renin expression [52, 53]. The renin gene initially translates preprorenin whose molecular weight is about 48 kDa. Once preprorenin translates, the "pre" signal peptide is going to be cleaved and prorenin is transported into endoplasmic reticulum. About 80% prorenin is released into circulation by various tissues through the constitutive secretory pathway. Circulated prorenin is inactive until it binds to specific membrane receptor and gains enzymatical activity which cleave angiotensinogen to angiotensin-I [54-56]. However, glycosylated prorenin is sorted into dense core vesicle and cleaved into active renin in JG cells [57].

The extracellular and intracellular signaling pathways which control the secretion and exocytosis of renin is very complicated. Three major extracellular pathways involved in renin production are renal sympathetic nerves, macula densa, and baroreceptor mechanism [58]. The renal sympathetic nerves release catecholamine which stimulates renin production by JG cell [59]. Macula densa senses the sodium depletion and enhances prostaglandins production which increase the renin synthesis by JG cells [60]. Integrin β1 as a baroreceptor which can senses perfusion pressure
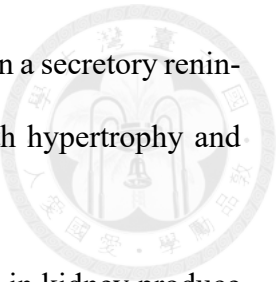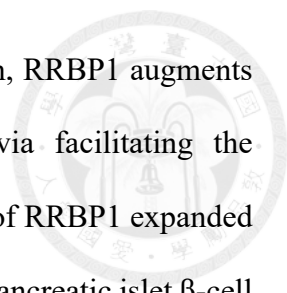
transmitted from extracellular matrix and induces renin gene expression by JG cell [61]. The extracellular pathways of renal sympathetic nerve and macula densa both increases cAMP which is a key regulator of renin production. cAMP is converted from adenosine triphosphate (ATP) by Adenylyl cyclase and is degraded by phosphodiesterases (PDE) [62]. cAMP can bind regulatory subunits of protein kinase A which phosphorylates CREB and further enhances renin expression [59]. cAMP also regulates renin release from granules of JG cells directly [63].

One of diseases derived from deficiency of renin is hyporeninemic hypoaldosteronism (HH). HH, also regarded as hyperkalemic RTA, is commonly found in a variety of renal diseases especially when due to diabetic nephropathy [64-66]. Generally, HH is asymptomatic until developing severe hyperkalemia which cause life-threatening arrhythmia [67-70]. Characteristic laboratory features of HH are decreased production of renin, aldosterone, and renin activity [65]. In turn, the excretion of potassium by the renal tubules is impaired in the HH patients [71]. Moreover, the HH patients can produce acidic urine since the reduced ammoniagenesis [65]. However, the pathogenesis of HH is due to damage to juxtaglomerular apparatus in which has specialized renin-producing cells, JG cells [72-73]. JG cells are specialized smooth muscle cells which mainly synthesize, store, secrete renin and mainly located in the media layer of afferent arterioles [42, 74-75].

1-5 RRBP1

RRBP1 (endoplasmic reticulum ribosomal-binding protein 1), also called p180 or ES/130, is an endoplasmic reticular transmembrane protein which interacts with ribosome. RRBP1 plays a crucial role in nascent protein translocation, transportation, and secretion. It is in charge of microtubules binding and bundling, which in turn regulates ER membrane proliferation and function as well. RRBP1 is also required to

terminal differentiation of secretory cell line [76-83]. In addition, RRBP1 augments the synthesis and secretion of procollagen by fibroblasts via facilitating the association of ER and ribosome [84]. However, overexpression of RRBP1 expanded ER membranes but did not increase the secretion of amylin in a pancreatic islet β-cell line [82].

1-6   Genetic variants of *RRBP1* in CVDs

There are some studies showed that RRBP1 variants are associated with coronary artery and arterial aneurysm, and vascular headache [85-87]. Moreover, RRBP1 facilitates the biogenesis of very-low-density lipoproteins (VLDL) through promoting rough ER wrapped closely to mitochondria which may increase the risk of CVD [88]. According to the above-mentioned descriptions, the role of RRPB1 in cardiovascular physiology and its relationship between the conversion and secretion of renin remain a lot of unclear.

In our laboratory, we initially made the groundbreaking discovery that a specific 7-SNP haplotype within the RRBP1 gene is strongly linked to lower systolic blood pressure (SBP), diastolic blood pressure (DBP), and mean blood pressure (MBP) in the Stanford Asia-Pacific Program for Hypertension and Insulin Resistance (SAPHHIRe) database. To further explore this association, we conducted in vivo studies using *Rrbp1*-knockout mice. These mice exhibited hypotension (low blood pressure) and increased mortality rates. Additionally, the *Rrbp1*-knockout mice displayed hyperkalemia (elevated potassium levels) and hyporeninemic hypoaldosteronism (reduced renin and aldosterone production) with higher levels of plasma angiotensinogen but lower levels of plasma renin, angiotensin-I (Ang-I), angiotensin-II (Ang-II), and aldosterone [113].

Under conditions of high potassium intake, *Rrbp1*-knockout mice experienced severe

hyperkalemia, arrhythmia, and a dramatic increase in mortality within a month. To further investigate the underlying mechanisms, we conducted in vitro studies using the Calu-6 cell line, wherein we knocked down RRBP1 expression. This knockdown resulted in reduced renin secretion but enhanced intracellular accumulation of renin. Moreover, the deficiency of RRBP1 impaired the transport of renin into the endoplasmic reticulum (ER) compartment, thereby affecting renin maturation and secretion in both mouse kidneys and cell-based experiments [113].

2. Results and Figure legends

2-1 Our study has reported significant associations between genetic variants of *RRBP1* and blood pressure.

Initially, our research group conducted a genome-wide linkage scan using data from the Stanford Asia-Pacific Program for Hypertension and Insulin Resistance (SAPPHIRe), which involved 360 nuclear families and 1,144 participants. This scan aimed to identify genetic loci associated with abnormal blood pressure. As a result, we mapped a quantitative trait locus on chromosome 20 between 14.7-18.3 Mb. To perform further fine-mapping within this region, we genotyped 51 single nucleotide polymorphisms (SNPs) across six genes: PCSK2, BFSP1, RRBP1, SNX5, OVOL2, and CSRP2BP.

Through sliding window analysis, we identified a 7-SNP haplotype within the RRBP1 gene that demonstrated a significant association with lower systolic blood pressure (SBP), diastolic blood pressure (DBP), and mean blood pressure (MBP). This particular haplotype, with a frequency of 0.161, included the SNP rs6080761. Specifically, it was associated with lower SBP (Z-score=-3.90, haplotype-specific P-value=9.6 x 10-5, global P value=3.5 x 10-5), lower DBP (Z-score=-3.796, haplotype-specific P-value=1.47 x 10-5, global P-value=8.2 x 10-5), and lower MBP (Z-score=-4.135, haplotype-specific P-value=3.6 x 10-5, global P-value=2.8 x 10-5) (refer to Table 1).

In addition, the intronic variant rs6080761 of RRBP1 showed an association with DBP (Z-score=-2.19, P-value=0.028) and a marginal association with MBP (Z-score=1.85, P-value=0.064) within the SAPPHIRe cohort. This variant was also associated with SBP (P-value=0.028) in the Genetic Epidemiology Network of Arteriopathy study (GENOA pha00309.1), which included 1,538 Caucasian
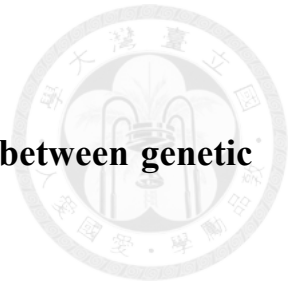
individuals. Furthermore, in the International Consortium for Blood Pressure study (ICBP pha003588) with 132,671 participants, rs6080761 was associated with DBP (P-value=0.013) and MBP (P-value=0.018). Similarly, in the National Heart, Lung, and Blood Institute (NHLBI, pha003048) Family Heart GWAS involving 2,756 participants, rs6080761 showed associations with DBP (P-value=0.01) and MBP (P-value=0.03) (refer to Table 1).

Table 1. The relationship between blood pressure and a 7-SNP haplotype (rs7272683, rs2236255, rs6034875, rs6080761, rs6080765, rs8120179, rs3790308) within the RRBP1 gene by FBAT analysis.

Haplotype	Freq	Number of informative families	SBP		DBP		MBP	
			Z	P [a]	Z	P [a]	Z	P [a]
H1: 2211111	0.211	91	1.043	0.297	0.755	0.450	0.963	0.335
H2: 2211121	0.161	78	-3.901	**0.000096**	-3.796	**0.000147**	-4.135	**0.000036**
H3: 2111111	0.131	62	1.652	0.099	1.470	0.142	1.648	0.099
H4: 1222211	0.079	45	1.260	0.208	1.853	0.064	1.793	0.073
H5: 2111121	0.071	46	-1.956	0.051	-0.785	0.433	-1.464	0.143
H6: 1122221	0.054	34	0.772	0.440	0.545	0.585	0.653	0.514
H7: 1222221	0.050	39	1.020	0.308	0.669	0.504	0.909	0.364
H8: 1122211	0.043	35	1.223	0.221	0.432	0.666	0.841	0.400
H9: 1211122	0.025	15	1.470	0.141	1.569	0.117	1.669	0.095
Global P-value [b]			**0.005288**		**0.020404**		**0.005116**	

FBAT, family-based association test; SNP, single nucleotide polymorphism; Freq, frequency; SBP, systolic blood pressure; DBP, diastolic blood pressure; MBP, mean blood pressure

2-2 Creation of *Rrbp1*-knockout mice.

To investigate the role of RRBP1 in blood pressure regulation, our research team generated *Rrbp1*-knockout mice. The experimental procedure involved the design of a vector plasmid containing a Frt neomycin resistance cassette flanked by loxP sites positioned between exon 3 and 4, as well as exon 24 and 25 of the *Rrbp1* gene (see Figure 1A). These *Rrbp1* floxed mice were then crossed with CMV-Cre mice to generate conventional knockout mice. Subsequent cross-breeding of heterozygous mice resulted in the production of *Rrbp1*-WT (wild-type), *Rrbp1*-HE (heterozygotes), and *Rrbp1*-knockout mice for use in subsequent experiments (refer to Figure 1B).

To evaluate the expression pattern of RRBP1, immunoblot assays were conducted using two different commercial antibodies. The results indicated that RRBP1 expression was predominantly observed in the intestine, kidney, liver, and pancreas in *Rrbp1*-WT mice (refer to Figure 1C).

A

B

C
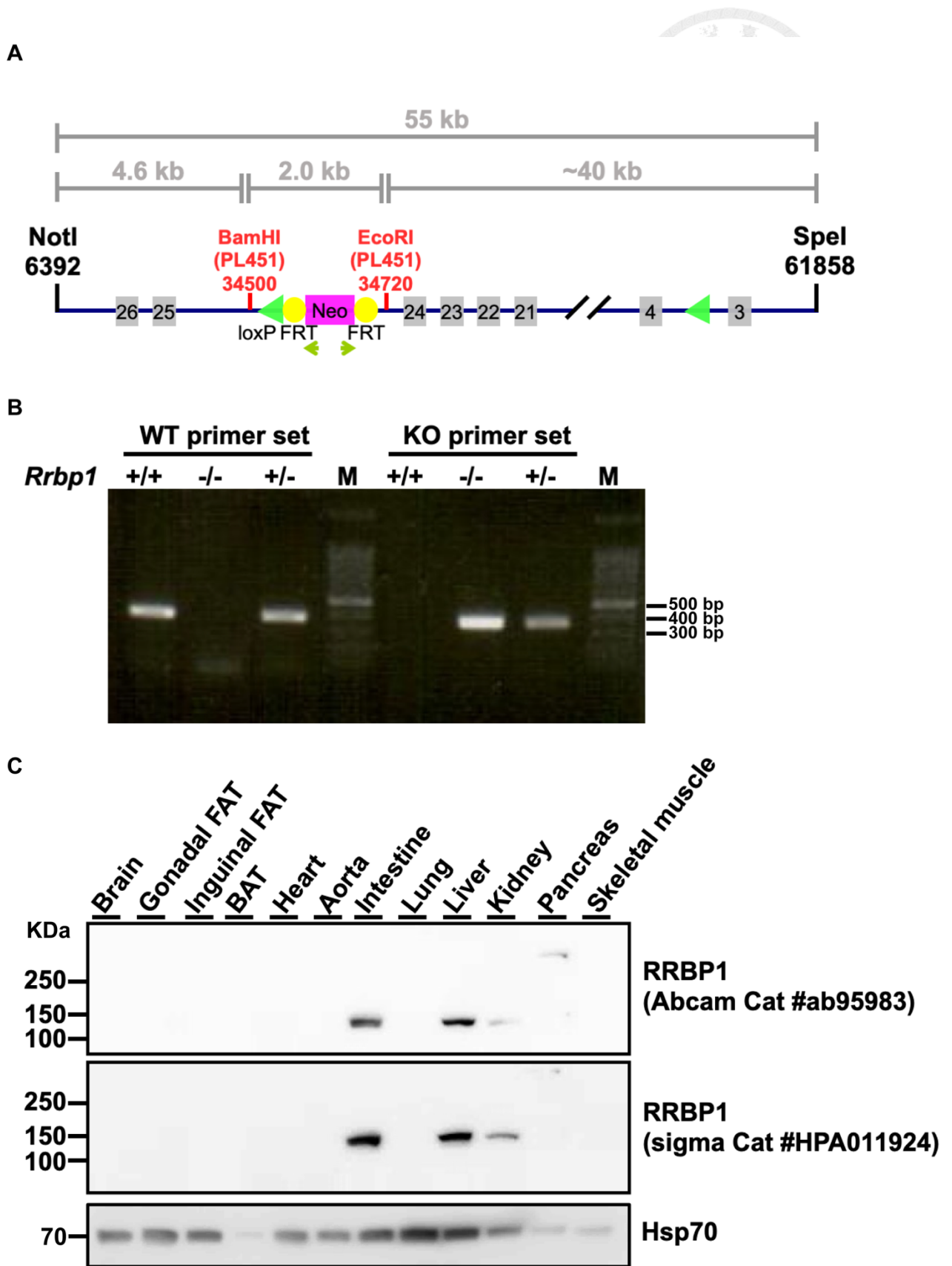
Figure 1. Creation of *Rrbp1*-knockout mice. (**A**) Schematic representation of the

Rrbp1-knockout construct. (**B**) Genotyping of *Rrbp1*-WT (+/+), *Rrbp1*-HE (+/-), and

Rrbp1-knockout (-/-) mice by PCR analysis. (**C**) The tissue distribution of RRBP1 by western blot assay in *Rrbp1*-WT mice. Lane1, brain; lane 2, gonadal white adipose tissue; lane 3, inguinal white adipose tissue; lane 4, brown adipose tissue; lane 5, heart; lane 6, aorta; lane 7, intestine; lane 8, lung; lane 9, liver; lane 10, kidney; lane 11, pancreas; and lane 12, skeletal muscle. WT, wild-type; HE, heterozygous; knockout, knock-out; Neo, neomycin; Frt, flanked neomycin resistant gene.

2-3 The basal phenotypes of *Rrbp1*-knockout mice.

The body length and size of 16 weeks-old *Rrbp1*-WT and *Rrbp1*-knockout mice showed no significantly different (Figure 2A-2B). There is also no difference in the anatomy between *Rrbp1*-WT and *Rrbp1*-knockout (Figure 2C-2D). To further characterize the body composition of *Rrbp1*-WT and *Rrbp1*-knockout mice, 16 weeks-old mice were conducted whole body scan using NMR spectroscopy. There is still no difference in body weight, body lean, body fat, and total body water between *Rrbp1*-WT and *Rrbp1*-knockout mice (Figure 2E-2H). Our group also weighed hearts, kidneys, livers, lungs, pancreas, spleen, and stomach. These tissues weights showed no difference between *Rrbp1*-WT and *Rrbp1*-knockout mice (Figure 2I-2O).
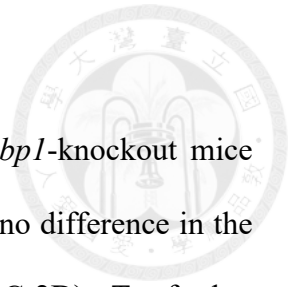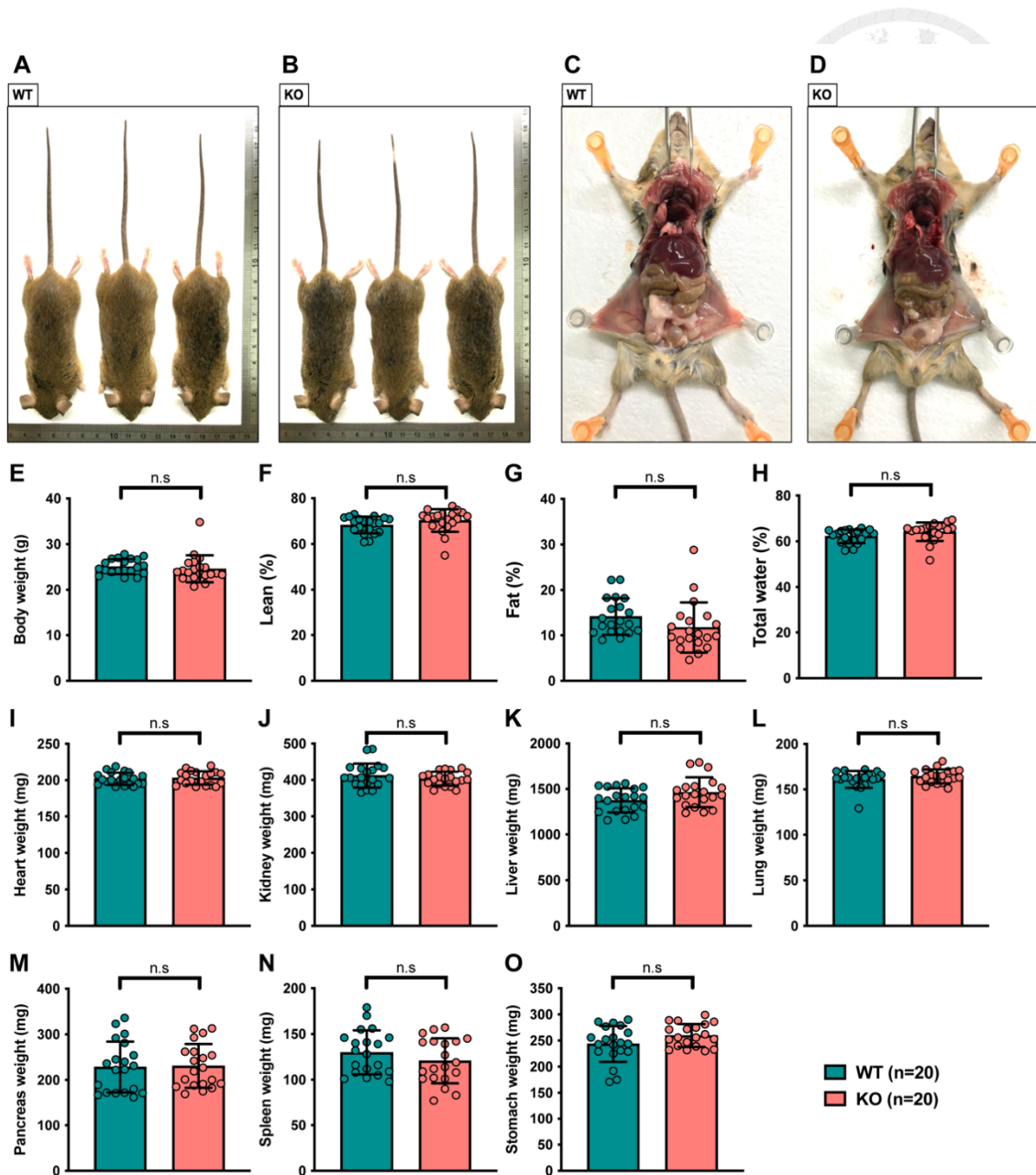
Figure 2. The basal phenotypes of *Rrbp1*-knockout mice. (A)-(B) The body size of *Rrbp1*-WT and *Rrbp1*-knockout was observed at 16 weeks old. **(C)-(D)** Abdominal anatomy of *Rrbp1*-WT and *Rrbp1*-knockout was dissected at 16 weeks old. **(E)-(H)** Body composition of 16-week-old *Rrbp1*-WT and *Rrbp1*-knockout mice including body weight, body lean, body fat, and total body water. **(I)-(O)** Tissues weights including heart, kidney, Liver, Lung, Pancreas, Spleen, and Stomach from *Rrbp1*-WT and *Rrbp1*-knockout mice.

2-4 The deficiency of RRBP1 in mice leads to lower blood pressure levels and an increased rate of sudden death.

To investigate the involvement of RRBP1 in blood pressure regulation, we measured the blood pressure of mice aged 10-16 weeks, including Rrbp1-WT, Rrbp1-HE, and Rrbp1-knockout mice. The results revealed a significant trend in decreasing systolic blood pressure among the three groups, with values of 112±2.94 mmHg for Rrbp1-WT, 103.8±2.12 mmHg for Rrbp1-HE, and 92.6±2.42 mmHg for Rrbp1-knockout mice (P-for-trend < 0.001) (see Figure 3A). Similarly, the diastolic blood pressure exhibited a decreasing trend, with values of 61.53±2.16 mmHg for Rrbp1-WT, 57.53±1.36 mmHg for Rrbp1-HE, and 48.94±2.31 mmHg for Rrbp1-knockout mice (P-for-trend < 0.01) (see Figure 3B).

Interestingly, our research group made an unexpected observation that Rrbp1-knockout mice showed an increased susceptibility to sudden death, irrespective of gender and age. This finding was supported by Kaplan-Meier survival curves, demonstrating a higher mortality rate in Rrbp1-knockout mice compared to Rrbp1-WT and Rrbp1-HE mice. Notably, Rrbp1-knockout mice had a shorter median lifespan (481 days) in comparison to Rrbp1-WT (793 days) and Rrbp1-HE (772 days) mice (see Figure 3C).

In order to understand the underlying cause of sudden death in Rrbp1-knockout mice, we monitored their cardiac rhythm using surface electrocardiography (ECG). The terminal ECG waveforms of Rrbp1-knockout mice exhibited characteristics consistent with severe hyperkalemia, including the presence of bizarre P waves, tall T waves, widening QRS complexes, and eventual asystole. To rule out the possibility of abnormal brain lesions as a cause of death, we conducted magnetic resonance imaging (MRI), which revealed no significant abnormalities (see Figure 3D-3P).

A P-for-trend<0.001

B P-for-trend<0.01

C
HR (WT vs. HE): 1.27 (95% CI 0.79-2.01, *P*= 0.55)
HR (WT vs. KO): 2.45 (95% CI 1.55-3.88, *P*< 0.0001)

WT (n=45)
HE (n=32)
KO (n=44)

D

WT #1

WT #2

0.5 mV
100 ms

KO #3

KO #4
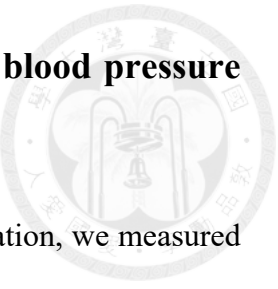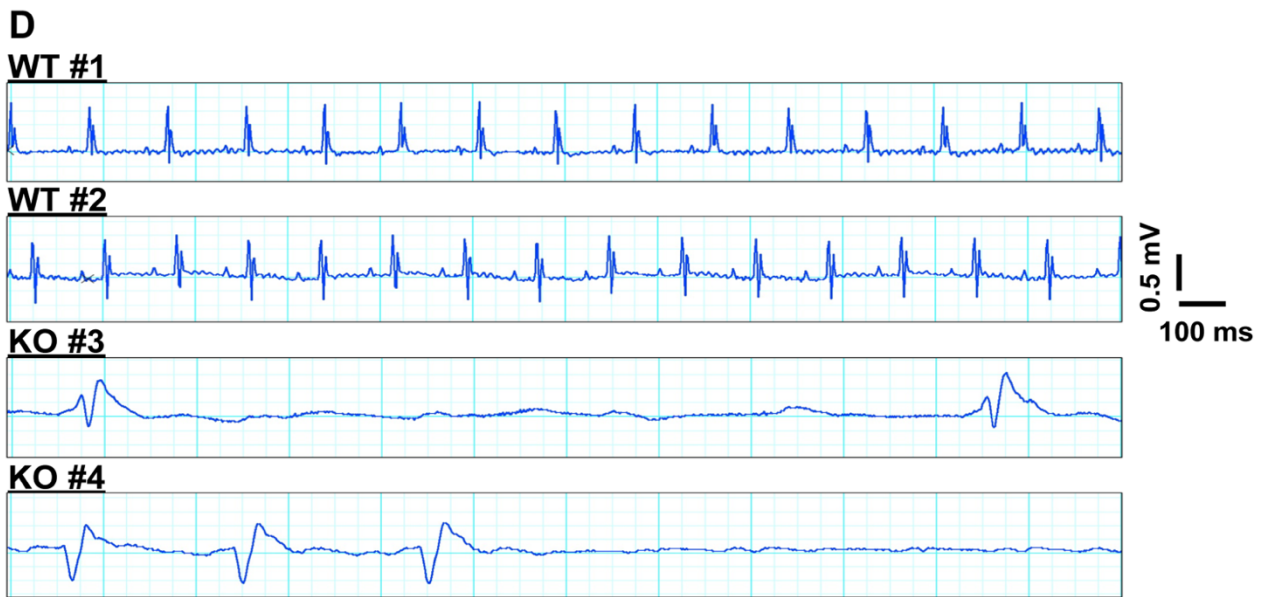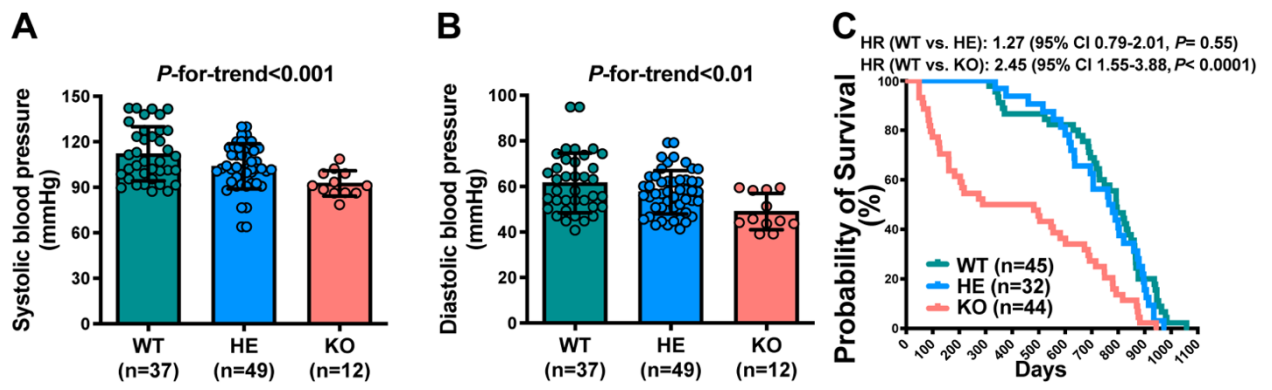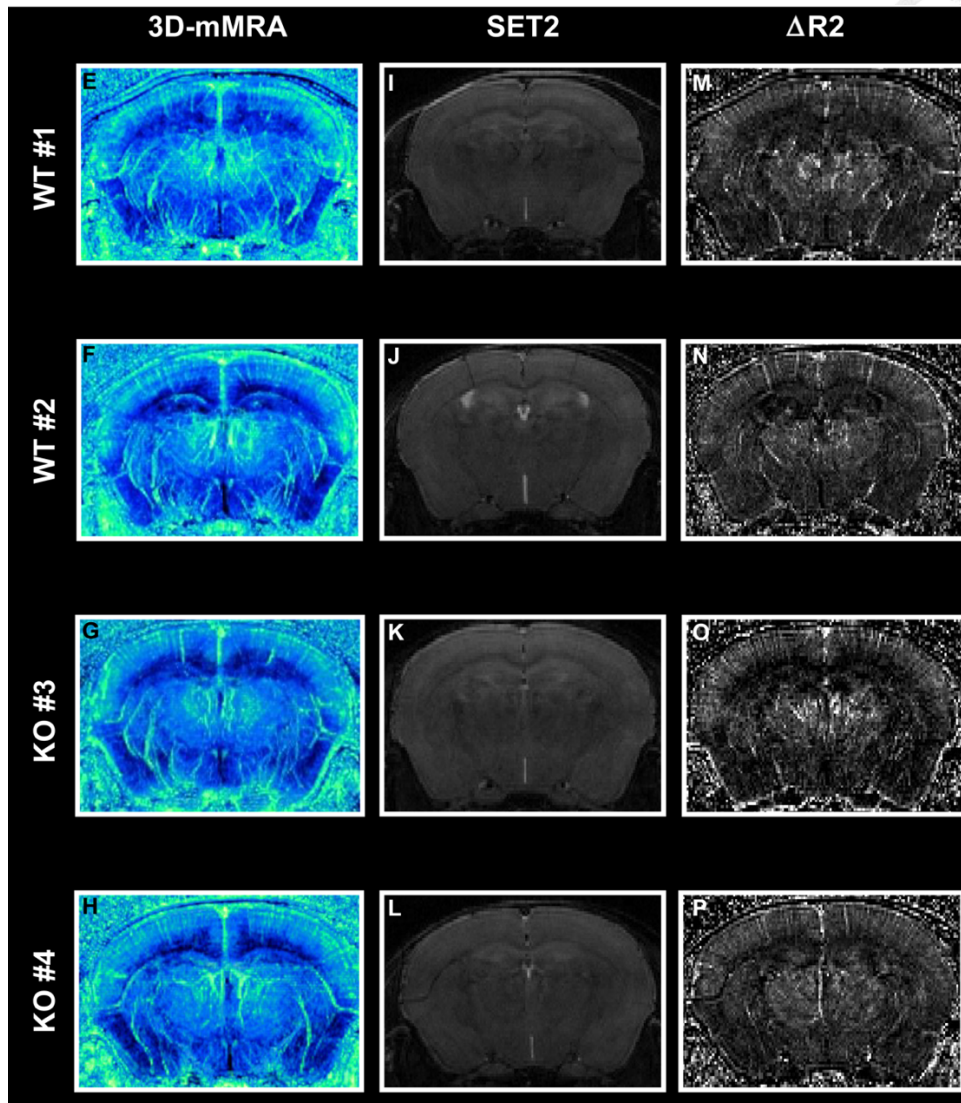
Figure 3. The blood pressure and survival rate of *Rrbp1*-knockout mice. (**A**) The systolic blood pressure of mice (**B**) The diastolic blood pressure of mice. Data represent mean ± SEM, n=12-49 per group. (**C**) Kaplan-Meier survival curve of *Rrbp1*-WT, *Rrbp1*-HE and *Rrbp1*-knockout mice. (**D**) The surface ECG waveform of *Rrbp1*-knockout and *Rrbp1*-WT mice. The ECG waveform of *Rrbp1*-WT mice #1 and #2. The terminal rhythms of *Rrbp1*-knockout mice #3 and #4. (**E**)-(**H**) 3-dimentioanl-ΔR2 micro magnetic resonance angiography of *Rrbp1*-WT and *Rrnp1*-knockout mice. (**I**)-(**L**) T$_1$-weighted images (T1WIs) of *Rrbp1*-WT and *Rrnp1*-knockout mice. (**M**)-(**P**) T$_2$-weighted images (T2WIs) of *Rrbp1*-WT and *Rrnp1*-knockout mice. WT, wild-type; HE, heterozygotes; knockout, knock-out.

2-5 The heart function and structure of *Rrbp1*-knockout mice display no significant difference compared with those of *Rrbp1*-WT mice.

In order to gain further insights into the cardiac function and structure of *Rrbp1*-WT and *Rrbp1*-knockout mice, our research team utilized echocardiography to assess the valves, chambers, and blood pumping. The results revealed several important findings. Firstly, the echocardiogram showed a lower cardiac output in *Rrbp1*-knockout mice compared to *Rrbp1*-WT mice (12.99±1.70 ml/min versus 15.63±1.83 ml/min; *P*-value=0.01) (see Figure 4A). Similarly, the stroke volume of *Rrbp1*-knockout mice was significantly reduced in comparison to Rrbp1-WT mice (43.65±5.55 μL versus 59.28±11.01 μL; *P*-value<0.01) (see Figure 4B). Furthermore, the left ventricular volume in diastole was also lower in *Rrbp1*-knockout mice compared to *Rrbp1*-WT mice (69.66±8.51 μL versus 92.26±21.56 μL; *P*-value=0.02) (see Figure 4C).

However, there were no significant differences observed between *Rrbp1*-WT and *Rrbp1*-knockout mice in terms of left ventricular mass, left ventricular posterior wall thickness, interventricular septum thickness in diastole, relative wall thickness, left ventricular fractional shortening, and left ventricular ejection fraction (see Figure 4D-4I). These findings suggest that while the cardiac output and stroke volume were reduced in *Rrbp1*-knockout mice, there were no changes observed in terms of wall thickness and contractility.

Overall, these results indicate that the lower blood pressure observed in Rrbp1-knockout mice can be attributed to a decrease in cardiac output and stroke volume, without significant alterations in wall thickness and contractility.
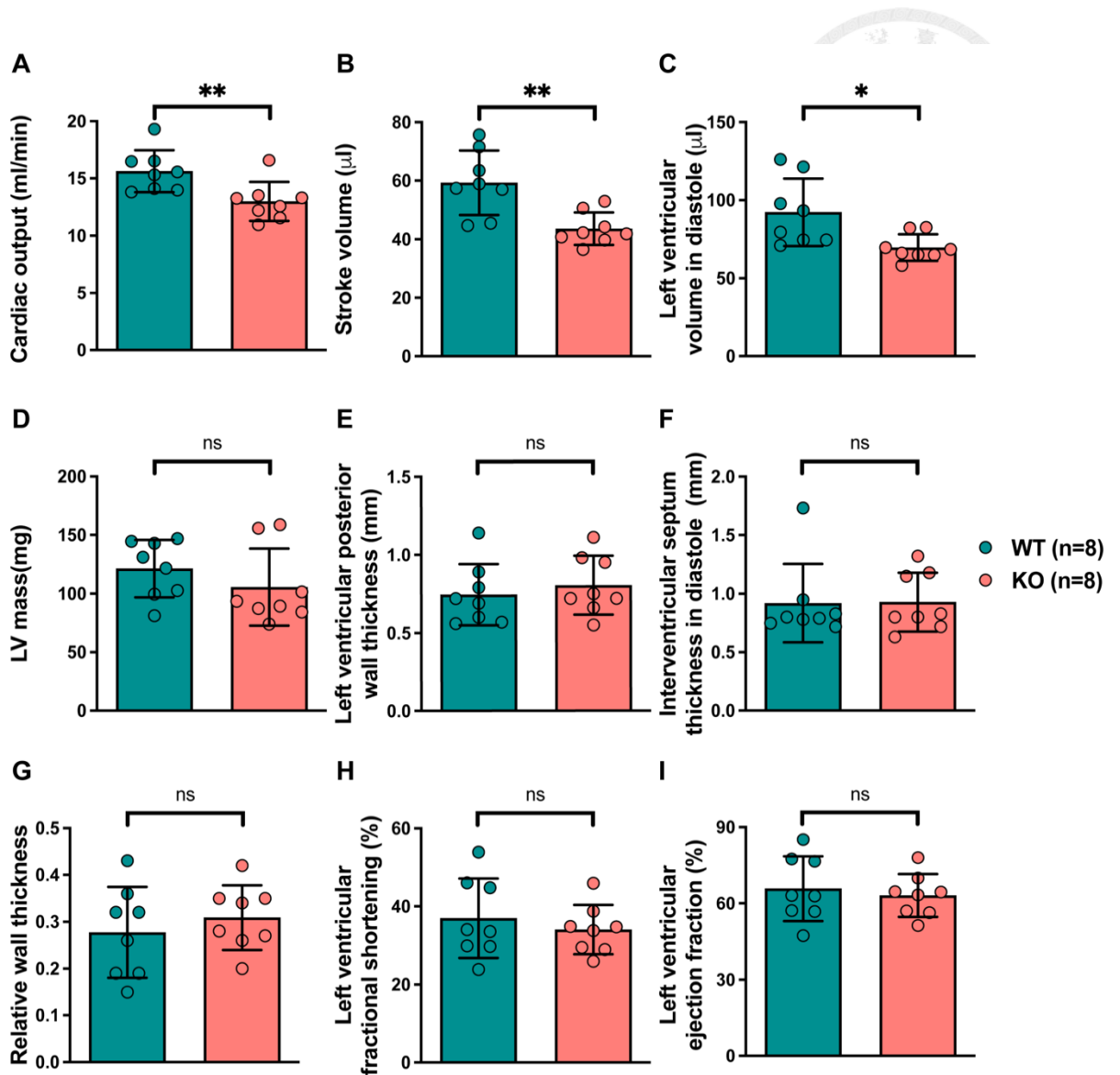
Figure 4. The echocardiogram analysis of mice. (**A**) The cardiac output; (**B**) the stroke volume; (**C**) the left ventricular volume in diastole; (**D**) the left ventricular mass; (**E**) the left ventricular posterior wall thickness; (**F**) the interventricular septum thickness in diastole; (**G**) the relative wall thickness in diastole; (**H**) the left ventricular fractional shortening; (**I**) the left ventricular ejection fraction measured by 2D-echocardiogram of *Rrbp1*-WT and *Rrbp1*-knockout mice. (n=8 per group) WT, wild-type; knockout, knock-out; LV, left ventricular. Data in A-I were analyzed with Student unpaired 2-tailed t test. Data were represented as mean ± SEM. ns, no significance; *P<0.05; ** P< 0.01

2-6 The basal plasma potassium level of *Rrbp1*-knockout mice is higher than that of control mice.

In light of the terminal ECG waveforms indicating severe hyperkalemia in *Rrbp1*-knockout mice, we proceeded to measure the levels of plasma and urine electrolytes in both *Rrbp1*-WT and *Rrbp1*-knockout mice aged between 10-16 weeks. The results provided noteworthy insights.

Firstly, we observed that the blood potassium level in *Rrbp1*-knockout mice was significantly higher compared to *Rrbp1*-WT mice (6.77 ± 0.14 mM versus 6.28 ± 0.11 mM; *P*-value<0.01). It is worth noting that the normal potassium level in C57BL/6 mice generally ranges between 4-5 mM, whereas our control mice (*Rrbp1*-WT) exhibited a slightly higher potassium level of approximately 6.28 mM. This discrepancy may be attributed to the mixed genetic background of C57BL6/129J, as described in the Materials and Methods section.

Furthermore, we evaluated the fractional excretion of potassium and found that it was significantly lower in *Rrbp1*-knockout mice compared to *Rrbp1*-WT mice (11.52 ± 0.843 versus 16.44 ± 0.997; *P*-value<0.001) (see Table 2). These findings suggest that *Rrbp1*-knockout mice have a diminished ability to excrete potassium, leading to hyperkalemia.

Overall, our results indicate that *Rrbp1*-knockout mice exhibit elevated levels of blood potassium and reduced potassium excretion, indicating a compromised ability to maintain potassium homeostasis and resulting in hyperkalemia.

Table 2. Plasma and urine electrolyte levels for *Rrbp1*-WT and *Rrbp1*-knockout mice.

Genotype (n)	*Rrbp1*-WT (n=21)	*Rrbp1*-knockout (n=16)
Blood		
[K^+], mmol/L	6.28±0.11	6.77±0.14 †
[Na^+], mmol/L	149.6±0.65	149.6±0.71
[Cl^-], mmol/L	113.9±0.59	113.9±0.59
Urine		
TTKG	9.5±0.1	9.1±0.2
FE_K^+	16.4±1.0	11.5±0.8 ‡
FE_{Na}^+	0.32±0.02	0.24±0.02 *
FE_{Cl}^-	0.70±0.04	0.56±0.05 *

TTKG, transtubular potassium gradient; FE, fractional excretion; *$P<0.05$, †$P<0.01$, ‡$P<0.001$ *Rrbp1*-knockout (knock-out) vs. *Rrbp1*-WT (wild-type)

2-7 The sudden death of *Rrbp1*-knockout mice increases dramatically under high K^+ intake within 30 days

To investigate the underlying causes of the increased sudden death observed in *Rrbp1*-knockout mice, we focused on the association between hyperkalemia and these fatal events. To this end, we subjected both *Rrbp1*-WT and *Rrbp1*-knockout mice to a high-potassium (K^+) diet and water for a duration of 30 days (Figure 5A).

Remarkably, the death events in *Rrbp1*-knockout mice exhibited a significant and dramatic increase within the 30-day period of high-K^+ intake (Figure 5B). As expected, the blood potassium levels in *Rrbp1*-knockout mice were significantly higher compared to *Rrbp1*-WT mice after 2 days of high-K^+ intake (8.53±0.38 versus 7.23±0.27 mmol/L; *P*-value=0.0086).

Consistently, we also observed lower transtubular potassium gradient (TTKG) values (14.62±0.79 versus 18.44±1.04; *P*-value=0.0058) and reduced urine fractional excretion of potassium (43.14±4% versus 64.84±6.7%; *P*-value=0.0081) in *Rrbp1*-knockout mice compared to *Rrbp1*-WT mice (see Table 3).

These findings provide compelling evidence that *Rrbp1*-knockout mice, when exposed to a high-K^+ diet, experience a substantial increase in sudden death events. Additionally, the observed hyperkalemia, lower TTKG values, and reduced urine fractional excretion of potassium in *Rrbp1*-knockout mice further support the impaired ability of these mice to regulate potassium levels.

In summary, our investigation highlights the crucial role of RRBP1 in maintaining potassium homeostasis, as *Rrbp1*-knockout mice exhibit a heightened susceptibility to sudden death when subjected to high-K^+ intake. The observed abnormalities in potassium levels and excretion mechanisms further emphasize the importance of RRBP1 in the regulation of potassium balance.
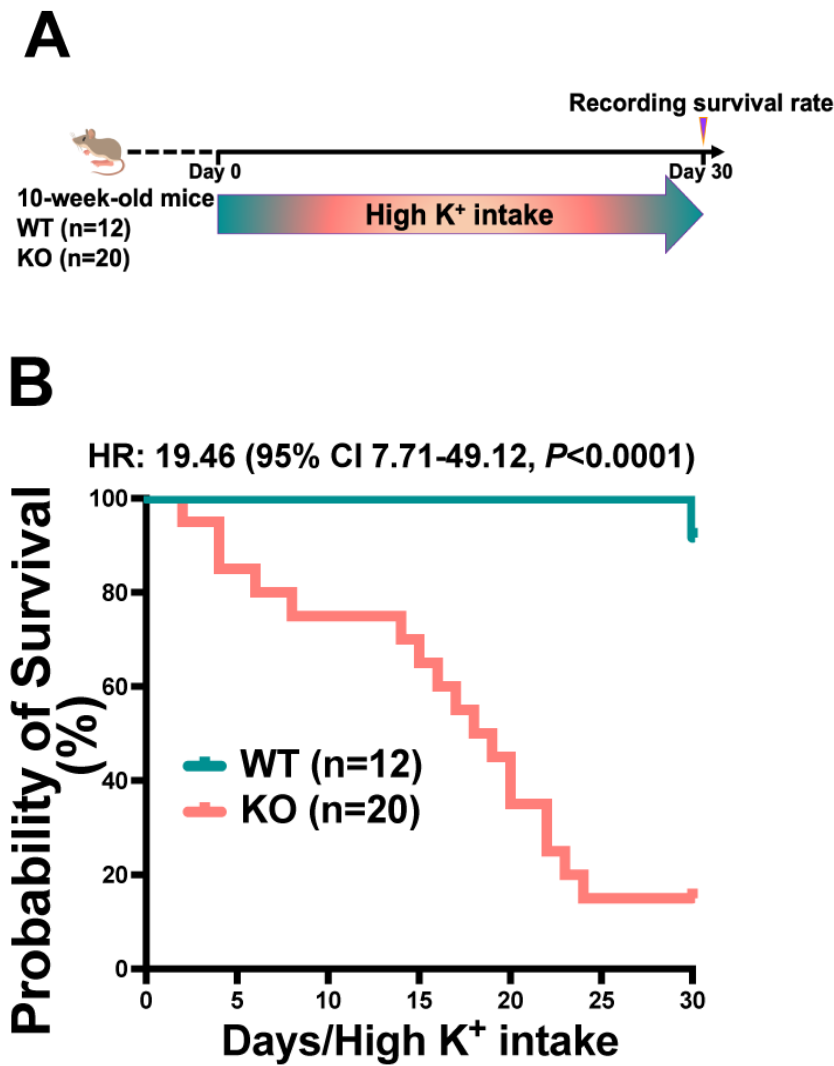
Figure 5. The survival rate of *Rrbp1*-WT and *Rrbp1*-knockout mice under high K⁺ intake. (**A**) Study protocol for recording the survival rate of mice under high K⁺ intake for a month. (**B**) Kaplan-Meier survival curve of *Rrbp1*-WT and *Rrbp1*-knockout mice under high K⁺ intake for 30 days.

Table 3. Plasma and urine electrolyte levels for *Rrbp1*-WT and *Rrbp1*-knockout mice under high K⁺ intake.

Genotype (n)	*Rrbp1*-WT (n=21)	*Rrbp1*-knockout (n=16)
Blood		
$[K^+]$, mmol/L	7.23±0.27	8.53±0.38 †
$[Na^+]$, mmol/L	157.7±1.32	155.9±1.62
$[Cl^-]$, mmol/L	122.6±1.61	123.4±2.03
Urine		
TTKG	18.4±1.0	14.6±0.8 †
FE_{K^+}	64.8±6.7	43.1±4.0 ‡
FE_{Na^+}	0.42±0.05	0.42±0.04
FE_{Cl^-}	3.24±0.33	2.63±0.27

TTKG, transtubular potassium gradient; FE, fractional excretion; *P<0.05, †P<0.01, ‡P<0.001 *Rrbp1*-knockout (knock-out) vs. *Rrbp1*-WT (wild-type)

2-8 The ECG waveform of *Rrbp1*-knockout mice is disturbed under high K$^+$ intake for 2 days.

To further elucidate the relationship between sudden death in *Rrbp1*-knockout mice and life-threatening arrhythmias resulting from hyperkalemia, we conducted cardiac rhythm monitoring using telemetry electrocardiography (ECG) on 12-16 weeks old *Rrbp1*-WT and *Rrbp1*-knockout mice before and after a two-day high-potassium (K$^+$) intake (Figure 6A).

Prior to the high K$^+$ intake, there were no significant differences in the RR interval, heart rate, PR interval, P duration, QRS interval, QT interval, corrected QT interval, T amplitude, and P amplitude between *Rrbp1*-WT and *Rrbp1*-knockout mice (Figure 6B-6J). However, following the two-day high K$^+$ intake, the PR interval (0.044±0.008 versus 0.034±0.003 secs; *P*-value<0.05), P duration (0.014±0.003 versus 0.010±0.001 secs; *P*-value<0.05), QRS interval (0.017±0.007 versus 0.011±0.001 secs; *P*-value<0.05), QT interval (0.036±0.005 versus 0.029±0.005 secs; *P*-value<0.05), and corrected QT interval (0.105±0.014 versus 0.093±0.016 secs; *P*-value<0.05) in *Rrbp1*-knockout mice were significantly longer compared to *Rrbp1*-WT mice (Figure 6D-6H).

After the two-day high K$^+$ intake, the RR interval, heart rate, T amplitude, and P amplitude of both *Rrbp1*-WT and *Rrbp1*-knockout mice showed no significant differences, although a trend was observed in the P values. Notably, two *Rrbp1*-knockout mice exhibited peaked T waves, a classical finding associated with severe hyperkalemia, which was not observed in *Rrbp1*-WT mice. The ECG waveforms of *Rrbp1*-WT and *Rrbp1*-knockout mice before and after the high K$^+$ intake were displayed below (Figure 6K).

These results provide further evidence linking the sudden death of *Rrbp1*-knockout

mice to the development of life-threatening arrhythmias, specifically associated with hyperkalemia. The prolonged PR interval, P duration, QRS interval, QT interval, and corrected QT interval observed in Rrbp1-knockout mice following high K^+ intake suggest a disruption in cardiac electrical conduction. The presence of peaked T waves in some *Rrbp1*-knockout mice further supports the association between hyperkalemia and the observed arrhythmias.

In summary, our findings highlight the role of RRBP1 in maintaining normal cardiac rhythm and preventing the occurrence of fatal arrhythmias, particularly in the context of hyperkalemia.
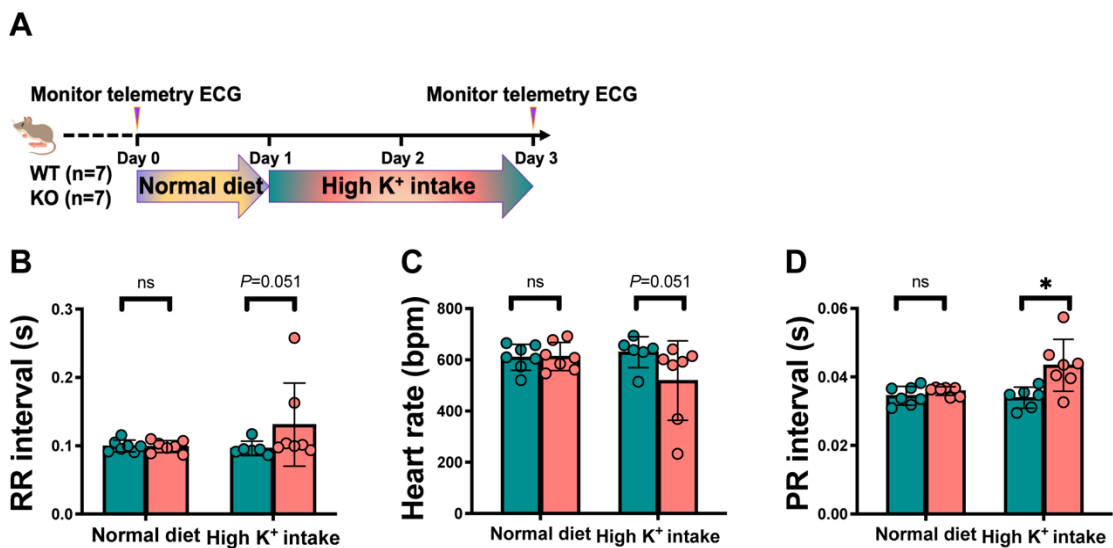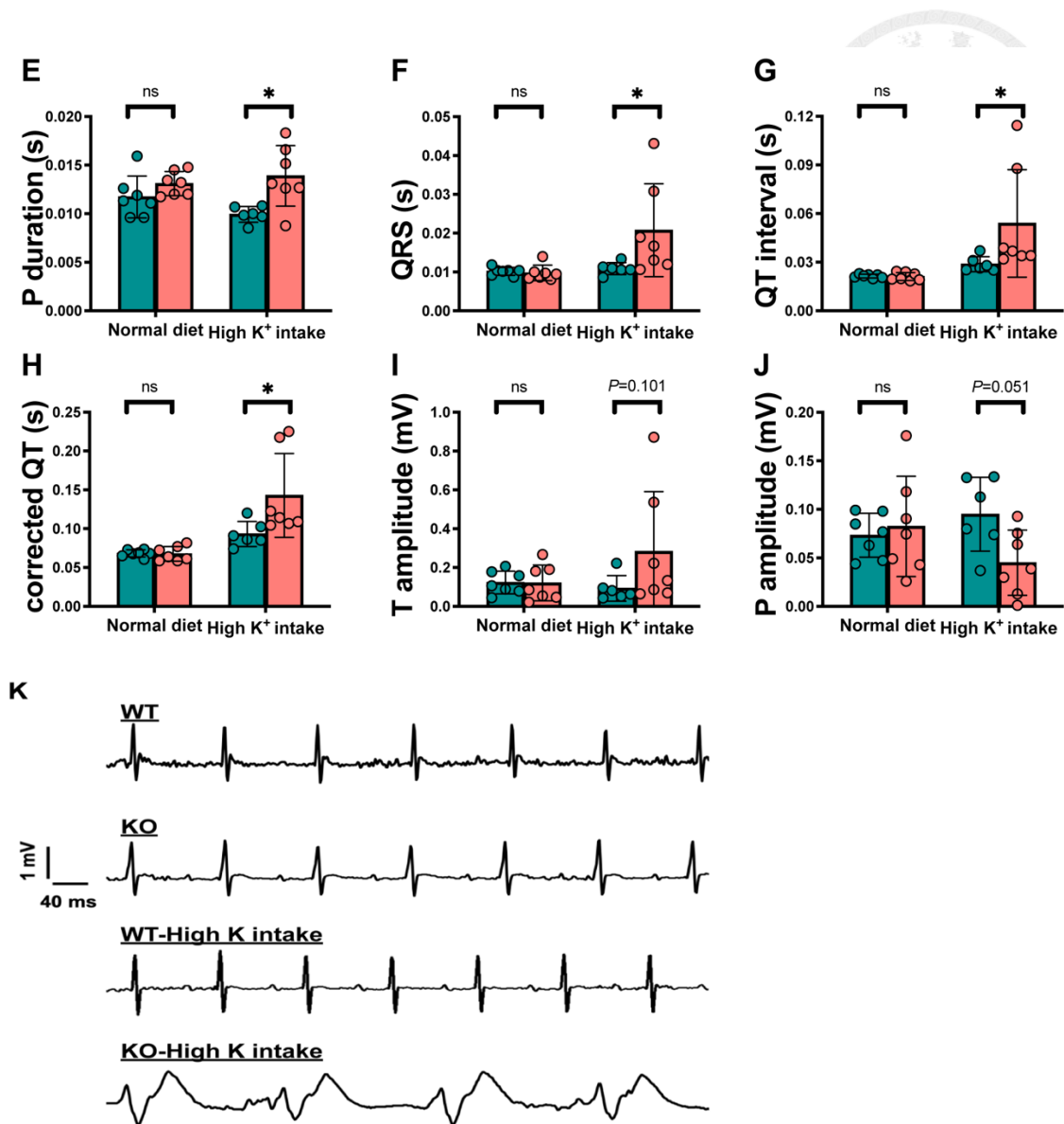
Figure 6. The telemetry ECG of *Rrbp1*-WT and *Rrbp1*-knockout mice before and after high K⁺ intake. (**A**) Experimental protocol of telemetry ECG monitoring on mice before and after high K⁺ intake. (**B**)-(**J**) Quantitation of telemetry ECG parameters in mice before and after high K⁺ intake. RR interval; heart rate; PR interval; P duration; QRS duration; QT interval; correct QT interval; T amplitude; P amplitude (n=6-7 per group). (**K**) The telemetric ECG waveforms of *Rrbp1*-WT and *Rrbp1*-knockout mice before and after high K+ intake for 2 days. WT, wild-type; knockout, knock-out. Data in B-J were analyzed with Mann-Whitney test. Data were represented as mean ± SEM. ns, no significance; *P<0.05

2-9 *Rrbp1*-knockout mice display hyporeninemic hypoaldosteronism.

To investigate the involvement of the renin-angiotensin-aldosterone system (RAAS) in the altered blood pressure and electrolyte balance observed in *Rrbp1*-knockout mice, we evaluated various components of the system. ELISA assays revealed that *Rrbp1*-knockout mice exhibited significantly higher levels of plasma angiotensinogen (49.72±12.53 versus 40.72±7.20 µg/ml; *P*-value=0.0001) (Figure 7A) compared to *Rrbp1*-WT mice. Conversely, the levels of plasma renin (28.21±2.47 versus 29.84±2.60 ng/ml; *P*-value=0.0059) (Figure 7B), angiotensin-I (172.7±63.5 versus 251.0±141.4 pg/ml; *P*-value=0.0016) (Figure 7C), angiotensin-II (343.2±203.8 versus 526.9±229.5 pg/ml; *P*-value=0.0017) (Figure 7D), and aldosterone (812.1±486.1 versus 1697.0±651.2 pg/ml; *P*-value<0.0001) (Figure 7E) were lower in *Rrbp1*-knockout mice compared to *Rrbp1*-WT mice.

Furthermore, the plasma renin activity of *Rrbp1*-knockout mice was significantly reduced (Figure 7F) (*P*-value<0.01). Immunoblotting analysis of kidney tissue from *Rrbp1*-knockout mice demonstrated decreased protein expression of serum/glucocorticoid regulated kinase 1 (SGK1) (Figure 7G, 7H). SGK1 is a crucial regulator induced by aldosterone and is involved in the regulation of various renal ion channels, such as the epithelial sodium channel (ENaC) and renal potassium channels (ROMK). Its activity enhances sodium reabsorption and potassium secretion [89].

Interestingly, the transcript levels of *Scnn1a*, which encodes ENaC-α protein, showed no significant difference between *Rrbp1*-knockout and *Rrbp1*-WT mice. However, the transcript levels of *Scnn1b*, *Scnn1g*, and *Kcnj1*, which encode ENaC-β, ENaC-γ, and ROMK, respectively, were lower in *Rrbp1*-knockout mice compared to *Rrbp1*-WT mice (Figure 7I).

These findings suggest that in *Rrbp1*-knockout mice, there is an imbalance in the

RAAS characterized by elevated angiotensinogen levels and decreased levels of renin, angiotensin-I, angiotensin-II, and aldosterone. The reduced plasma renin activity further supports this dysregulation. Additionally, the decreased expression of SGK1 and altered transcript levels of *Scnn1b*, *Scnn1g*, and *Kcnj1* indicate disrupted renal ion channel regulation in *Rrbp1*-knockout mice.

Taken together, these results provide insights into the involvement of the RAAS in the observed lower blood pressure and altered electrolyte balance in Rrbp1-knockout mice. The dysregulated RAAS components likely contribute to the physiological abnormalities observed in these mice.
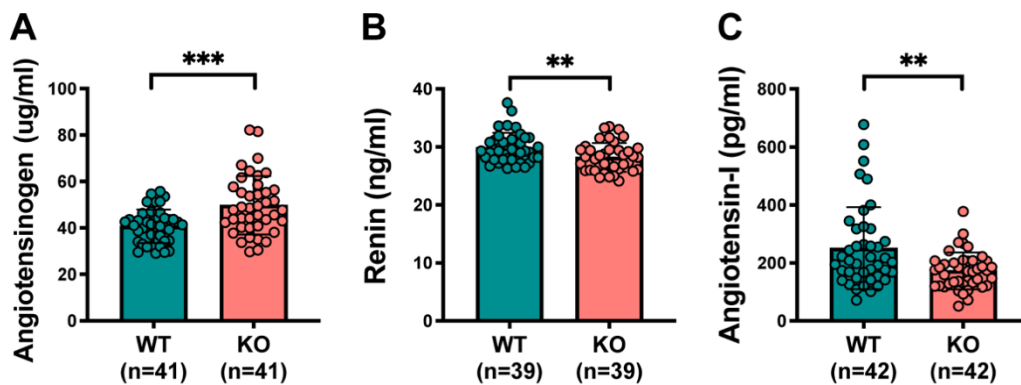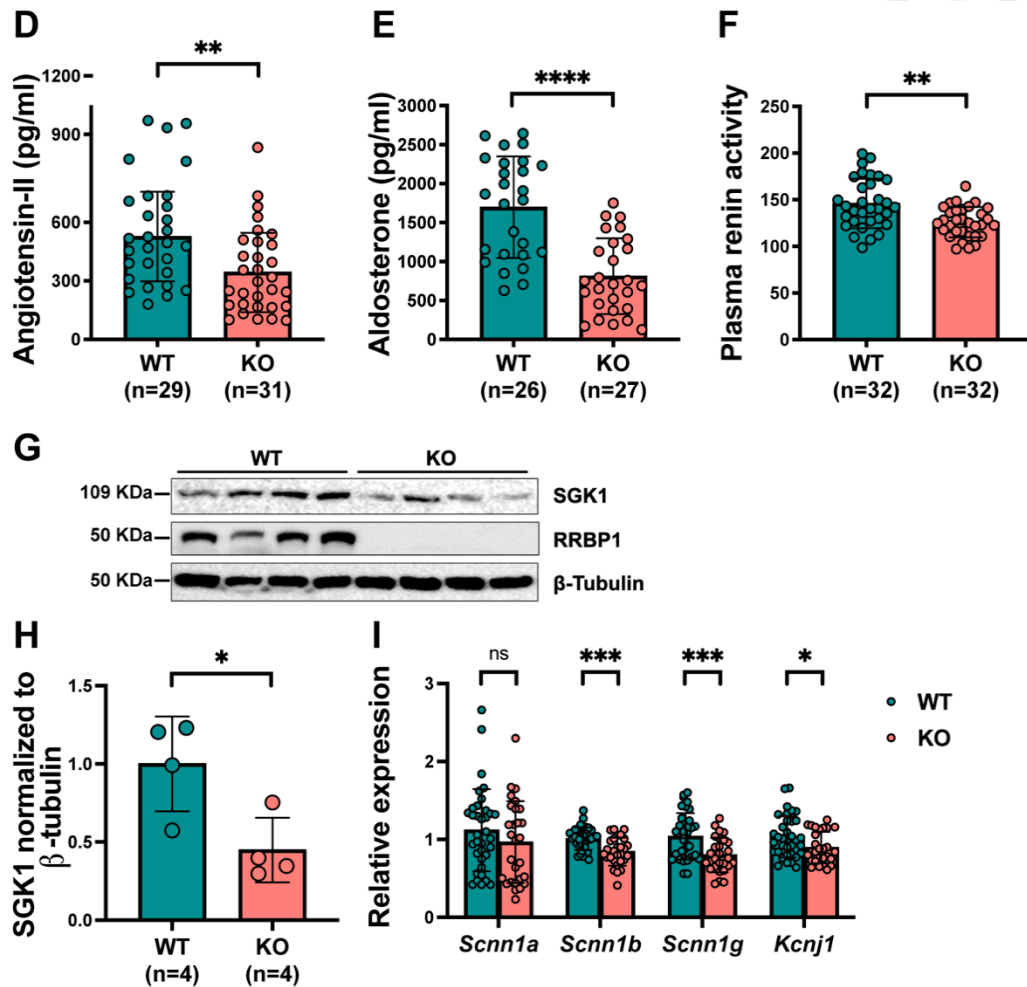
Figure 7. Hyporeninemic hypoaldosteronism of *Rrbp1*-knockout mice. (**A**) The plasma angiotensinogen level; (**B**) the plasma renin; (**C**) the plasma Ang-I; (**D**) the plasma Ang-II; (**E**) the plasma aldosterone level and (**F**) the plasma renin activity in mice. (**G**) SGK1 protein expression in kidneys of *Rrbp1*-WT and *Rrbp1*-knockout mice by western blots. (**H**) Quantification of the immunoblot in (**G**). (**I**) The transcripts levels of *Scnn1a*, *Scnn1b*, *Scnn1g*, and *Kcnj1* in kidney of *Rrbp1*-WT and *Rrbp1*-knockout mice using quantitative RT-PCR. Data were analyzed using the 2 - ΔΔCt method with GAPDH as the reference gene (n=28-35 per group). WT, wild-type; knockout, knock-out. Data in A-F,and I were analyzed with Student unpaired 2-tailed t test; data in h with were analyzed Mann-Whitney test. Data were represented as mean ± SEM. ns, no significance; * *P*-value<0.05; ** *P*-value< 0.01; *** *P*-value<0.001; **** *P*-value<0.0001

2-10 The adrenal gland function of *Rrbp1*-knockout mice has no significant difference with that of *Rrbp1*-WT mice.

To investigate the adrenal gland function in relation to the lower plasma aldosterone levels observed in *Rrbp1*-knockout mice, we performed tissue dissection and an adrenocorticotropic hormone (ACTH) stimulation test. Hematoxylin and eosin staining of the adrenal glands revealed no noticeable lesions in both *Rrbp1*-WT and *Rrbp1*-knockout mice (Figure 8A, 8B). Additionally, there were no significant differences in the weight of the adrenal glands between the two groups (Figure 8C).

To assess adrenal gland function, we conducted an ACTH stimulation test, a widely used method to determine adrenal responsiveness. We observed lower basal plasma levels of corticosterone in *Rrbp1*-knockout mice, which is consistent with the lower plasma angiotensin-II levels found in these mice. However, after ACTH injection for 30, 60, and 90 minutes, the plasma corticosterone levels increased in both *Rrbp1*-WT and *Rrbp1*-knockout mice, with no significant difference between the two groups (Figure 8D, 8E).

These results indicate that the adrenal glands of *Rrbp1*-knockout mice exhibit a normal response to ACTH stimulation, suggesting that their adrenal function is comparable to that of *Rrbp1*-WT mice. Furthermore, the absence of observable lesions and similar adrenal weight in *Rrbp1*-knockout mice further support the normal functioning of the adrenal glands in these mice.

In summary, our findings demonstrate that despite the lower basal plasma aldosterone levels, the adrenal glands of *Rrbp1*-knockout mice respond adequately to ACTH stimulation, indicating intact adrenal function in these mice.
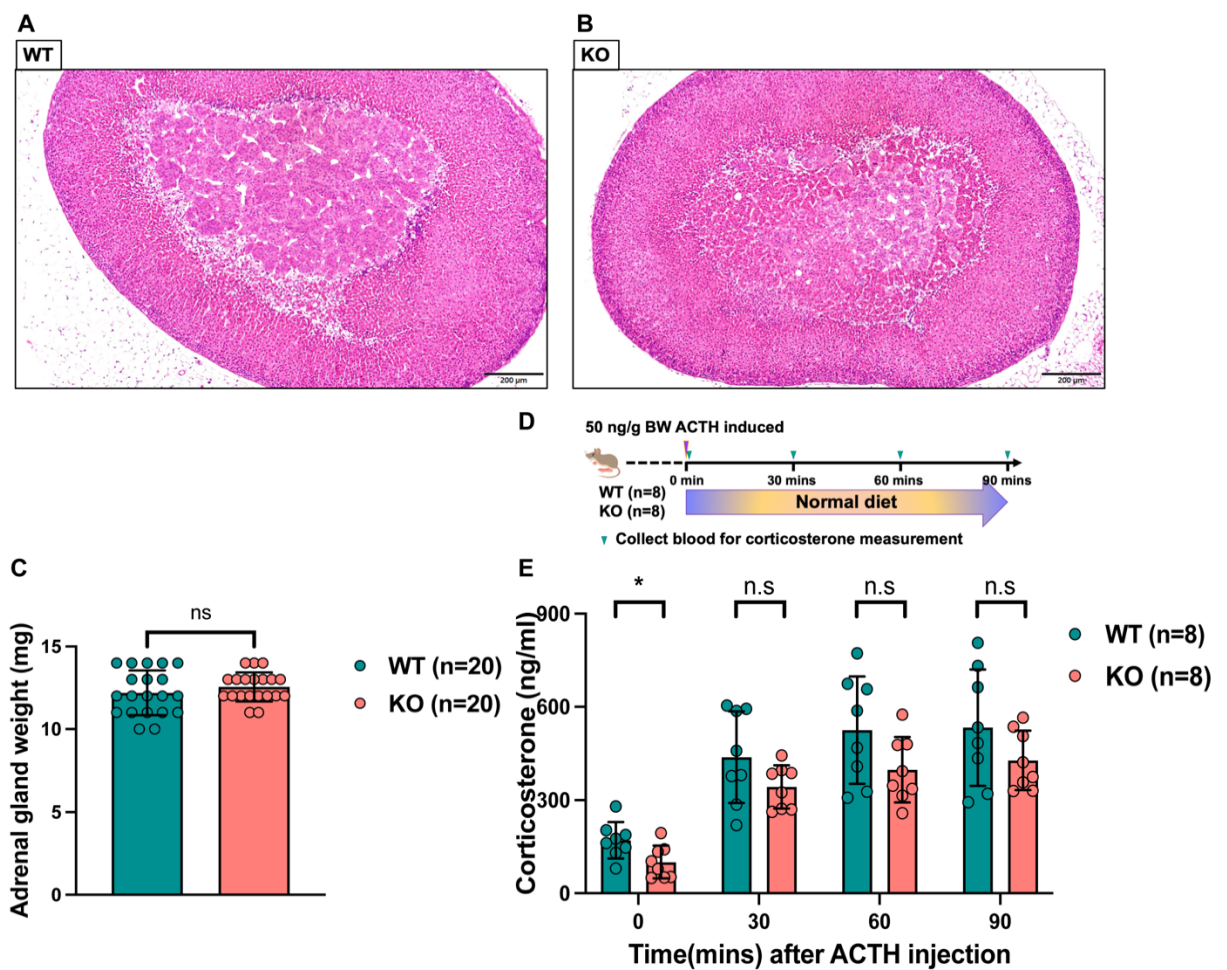
Figure 8. The adrenal function of *Rrbp1*-knockout mice. (**A**)-(**B**) The hematoxylin and eosin staining of adrenal gland in 16 weeks old *Rrbp1*-WT and *Rrbp1*-knockout. (**C**) Total adrenal gland weight of Rrbp1-WT and Rrbp1-knockout mice. (D) Experimental protocol for ACTH stimulation test of mice. (**E**) The plasma corticosterone level of *Rrbp1*-WT and *Rrbp1*-knockout mice after ACTH treatment after 0, 30, 60, and 90 minutes. WT, wild-type; knockout, knock-out. Data in (**C**) and (**E**) were analyzed with Student unpaired 2-tailed t test. Data were represented as mean ± SEM. ns, no significance; *P<0.05

2-11 The plasma renin, angiotensin-II, and aldosterone are still lower in *Rrbp1*-knockout mice under high K$^+$ intake for 2 days

To further investigate the impact of high potassium (K$^+$) intake on the renin-angiotensin-aldosterone system (RAAS) in *Rrbp1*-knockout mice, we examined the levels of RAAS components in mice subjected to high K$^+$ intake (Figure 9A). Interestingly, *Rrbp1*-knockout mice displayed lower plasma levels of renin (18.12±1.08 versus 19.51±1.601 ng/ml; *P*-value=0.024) (Figure 9B), angiotensin-II (855.7±310.8 versus 1365±803.5 pg/ml; *P*-value=0.015) (Figure 9C), and aldosterone (3361±826.2 versus 4397±1370 pg/ml; *P*-value=0.035) (Figure 9D) compared to *Rrbp1*-WT mice.

These findings indicate that under conditions of high K$^+$ intake, *Rrbp1*-knockout mice exhibit reduced levels of key components of the RAAS, including renin, angiotensin-II, and aldosterone, when compared to *Rrbp1*-WT mice. The decreased levels of renin, angiotensin-II, and aldosterone suggest a dysregulation of the RAAS in *Rrbp1*-knockout mice, which may contribute to the observed severe hyperkalemia and the development of life-threatening arrhythmias following high K$^+$ intake for 2 days.

In summary, our results demonstrate a disruption in the RAAS system in *Rrbp1*-knockout mice exposed to high K$^+$ intake, characterized by lower plasma levels of renin, angiotensin-II, and aldosterone compared to *Rrbp1*-WT mice. These findings provide further insight into the mechanisms underlying the severe hyperkalemia and hyperkalemic life-threatening arrhythmias observed in *Rrbp1*-knockout mice under high K$^+$ conditions.

Figure 9. The RAAS level of *Rrbp1*-knockout mice under high K⁺ intake for 2 days. (**A**) Experimental protocol for measurement of mice plasma RAAS level under high K+ intake. (**B**) The plasma renin; (**C**) the plasma Ang-II; and (**D**) the plasma aldosterone levels in mice under high K+ intake for 2 days. WT, wild-type; knockout, knock-out. Data in (**B**)-(**D**) were analyzed with Student unpaired 2-tailed t test. Data were represented as mean ± SEM. ns, no significance; *P<0.05
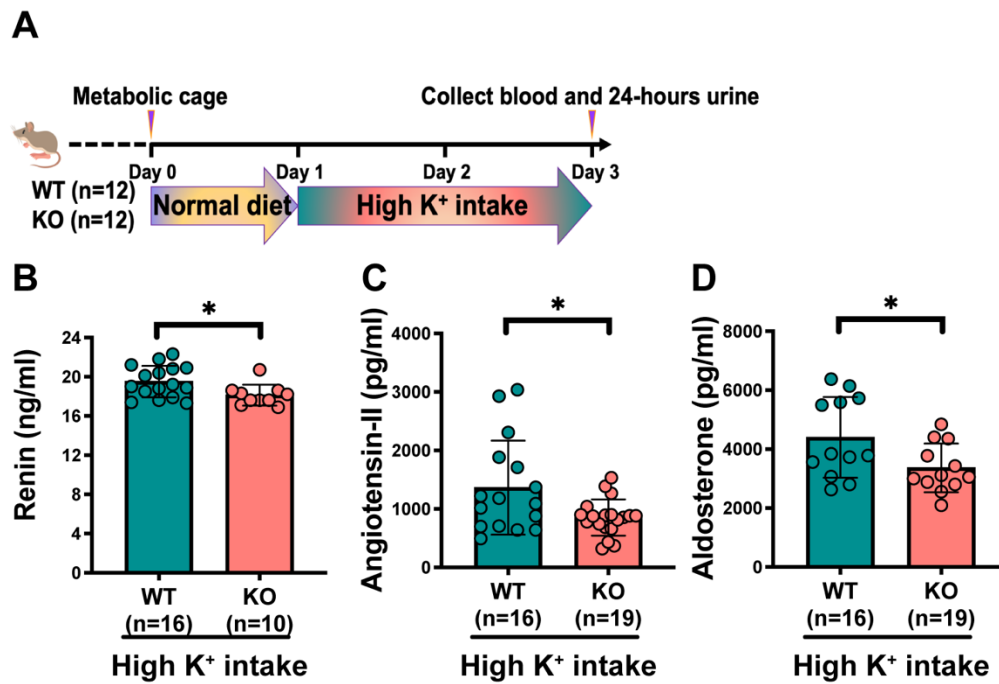
2-12 High K$^+$ load-induced hyperkalemia and sudden death in *Rrbp1*-knockout mice can be rescued by fludrocortisone treatment.

In this experiment, we aimed to strengthen our understanding of the role of the renin-angiotensin-aldosterone system (RAAS) in high-potassium (K$^+$) load-induced sudden death. To achieve this, we conducted a study involving mice.

Firstly, we administered a synthetic mineralocorticoid called fludrocortisone to the mice. The mice were divided into three groups: one group received a placebo (0 mg/kg), another group received a low dose of fludrocortisone (2.5 mg/kg), and the third group received a high dose of fludrocortisone (10 mg/kg). These treatments were administered through intraperitoneal injections once every two days for a total of 30 days.

The purpose of this treatment was to confirm whether the suppression of the RAAS is the primary cause of high-potassium load-induced sudden death. Figure 10A illustrates the findings of this experiment.

Additionally, we observed the survival rate of mice with a knockout of the *Rrbp1* gene (*Rrbp1*-knockout mice) when subjected to high-potassium intake. We found that the survival rate of these mice increased in a dose-dependent manner with the administration of fludrocortisone, as shown in Figure 10B.

To further investigate the effects of fludrocortisone treatment, we analyzed various parameters. Specifically, we measured the levels of sodium, potassium, and chloride in the mice's plasma, as well as the excretion of urinary potassium. Our results, presented in Table 4, indicated that there were no significant differences in these parameters when mice were subjected to high-potassium loading and treated with fludrocortisone.

In summary, our study involved treating mice with fludrocortisone to examine the

impact of RAAS suppression on high-potassium load-induced sudden death. The survival rate of *Rrbp1*-knockout mice increased in a dose-dependent manner with fludrocortisone treatment. Furthermore, no significant differences were observed in the levels of plasma sodium, potassium, chloride, and urinary potassium excretion in mice subjected to high-potassium loading and treated with fludrocortisone. These findings provide further support for the involvement of RAAS suppression in high potassium load induced sudden death.
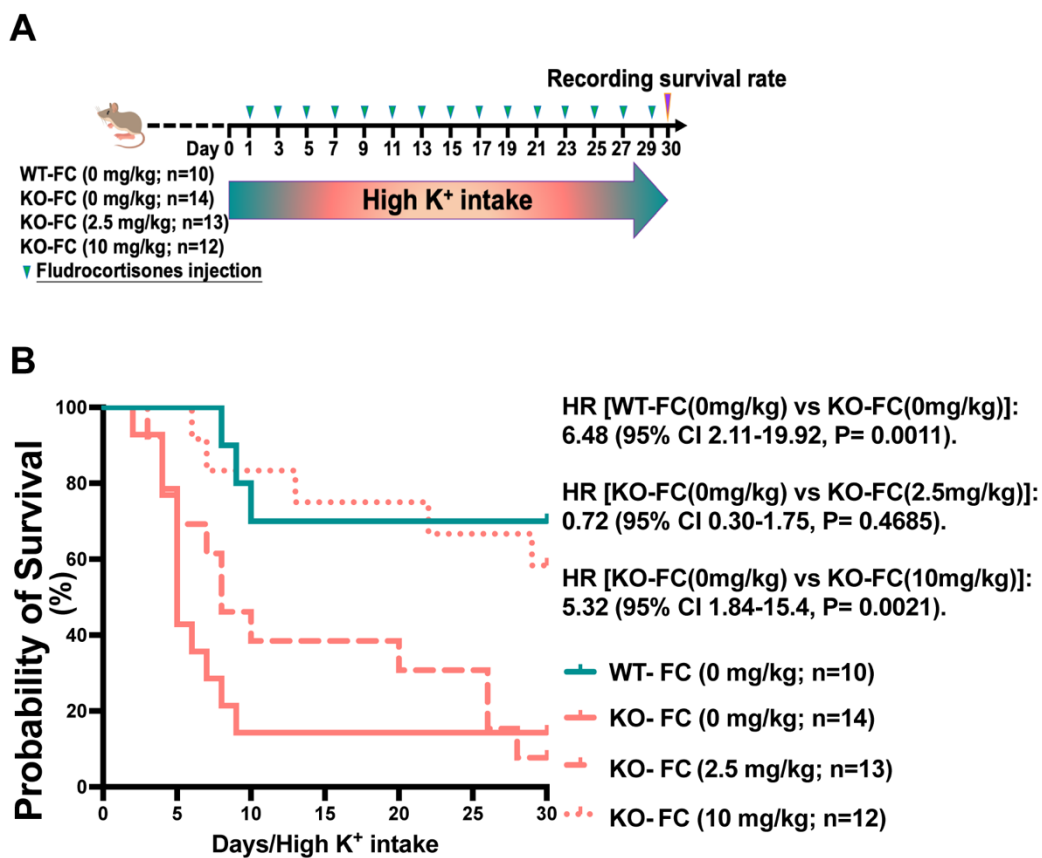
Figure 10. The survival rate of *Rrbp1*-knockout mice under high K$^+$ intake with Fludrocortisone treatment. (**A**) Experimental protocol of 0, 2.5, 10 mg/kg fludrocortisone treatment on mice under high K$^+$ intake for 30 days. (**B**) The survival curve of *Rrbp1*-WT and *Rrbp1*-knockout mice under high K$^+$ intake rescued with 0, 2.5, 10 mg/kg fludrocortisone treatment. WT, wild-type; knockout, knock-out; FC, fludrocortisone treatment. Data in (**B**) were analyzed with log-rank test.

Table 4. Plasma and urine electrolyte levels for *Rrbp1*-WT and *Rrbp1*-knockout mice under high K$^+$ intake for 48 hours with and without fludrocortisone treatment.

Genotype + treatment (n)	*Rrbp1*-WT + saline (n=22)	*Rrbp1*-knockout + saline (n=27)	*Rrbp1*-knockout + Fludrocortisone (n=18)
Blood			
[K$^+$], mmol/L	7.49±0.10	8.19±0.14 ‡	7.73±0.16
[Na$^+$], mmol/L	161.5±1.10	163.6±0.72	161.6±0.88
[Cl$^-$], mmol/L	124.6±0.99	127.1±0.77	124.6±1.35
Urine			
TTKG	29.9±1.1	30.2±1.3	30.6±1.6
FE$_K$$^+$	25.3±3.4	27.8±2.9	20.9±3.6
FE$_{Na}$$^+$	0.62±0.09	0.65±0.06	0.48±0.07
FE$_{Cl}$$^-$	1.15±0.17	1.39±0.15	0.98±0.15

TTKG, transtubular potassium gradient; FE, fractional excretion; *P<0.05, †P<0.01, ‡P<0.001 *Rrbp1*-knockout (knock-out) vs. *Rrbp1*-WT (wild-type)

2-13 The expression of renin is higher within the kidney section of *Rrbp1*-knockout mice.

In this part of our study, we focused on investigating the expression of renin within the kidneys of *Rrbp1*-knockout mice compared to *Rrbp1*-WT (wild-type) mice. Renin is an important component of the renin-angiotensin-aldosterone system (RAAS) involved in blood pressure regulation.

To assess the expression of renin, we employed immunohistochemical staining with an anti-renin antibody. This staining technique allowed us to visualize and compare the levels of renin in kidney sections of both types of mice. Figure 11A and 11B depict representative images of the immunohistochemical staining for renin in *Rrbp1*-knockout and *Rrbp1*-WT mice, respectively.

Interestingly, our analysis revealed a surprising finding. The intensity of the renin signal was significantly stronger in the kidney sections of *Rrbp1*-knockout mice compared to *Rrbp1*-WT mice. The mean intensity of renin signal in *Rrbp1*-knockout mice was 15.35 ± 2.93 arbitrary units, while it was 14.51 ± 1.62 arbitrary units in *Rrbp1*-WT mice. This difference in intensity was statistically significant ($P<0.05$), as shown in Figure 11C.

Overall, our immunohistochemical staining results indicate that *Rrbp1*-knockout mice exhibited a higher intensity of renin signal within their kidneys compared to *Rrbp1*-WT mice. This finding suggests a potential role of RRBP1 in the regulation of renin expression in the kidney and provides further insights into the involvement of the RAAS in our study.
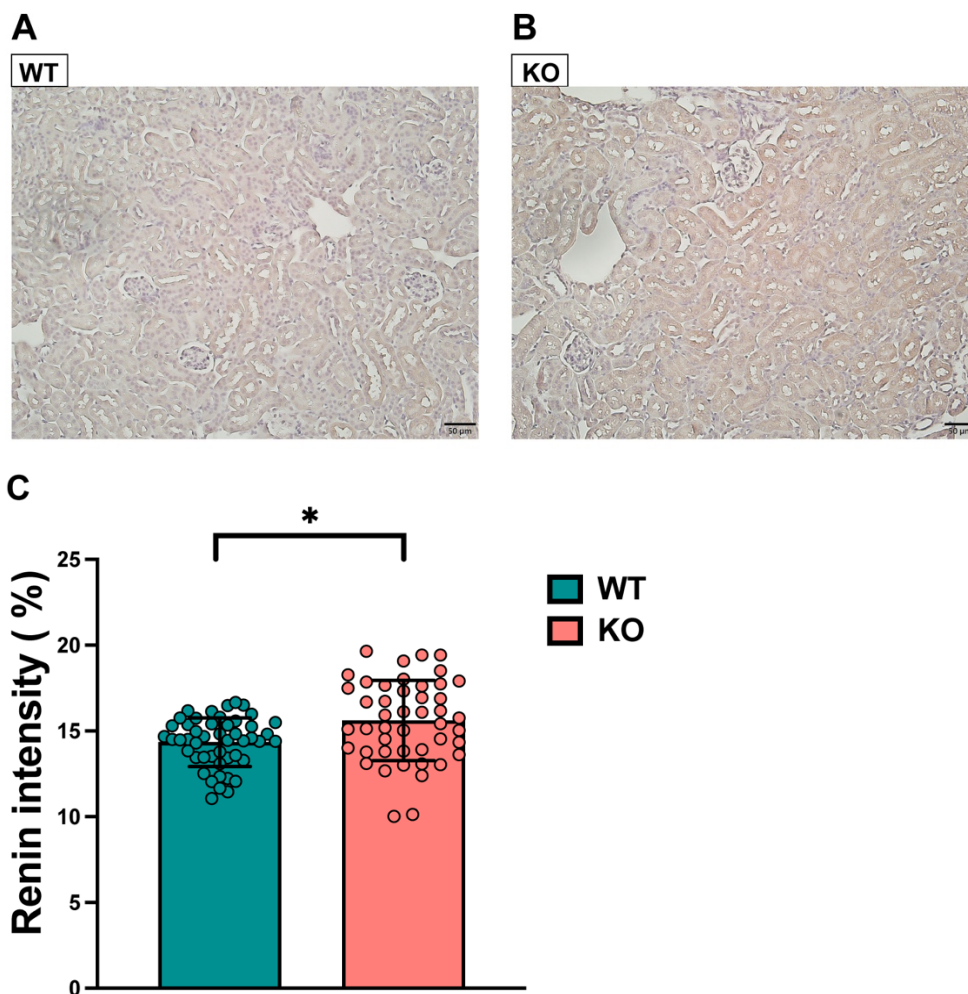
Figure 11. The renin intensity in the kidney sections of *Rrbp1*-WT and *Rrbp1*-knockout mice. (**A**)-(**B**) Renin immunohistochemical staining of kidneys of *Rrbp1*-WT and *Rrbp1*-knockout mice. (**C**) Quantification of stain intensity in kidneys from *Rrbp1*-WT and *Rrbp1*-knockout mice (scale bar= 20 μm). WT, wild-type; knockout, knock-out. Data in (**C**) were analyzed with Student unpaired 2-tailed t test. Data were represented as mean ± SEM. *P<0.05

2-14 The higher expression of intracellular renin and lower of secreted renin of *RRBP1*-KD cells.

In this particular phase of our research, we aimed to gain a better understanding of the role of RRBP1 (Ribosome Binding Protein 1) in the expression of renin. To accomplish this, we conducted experiments using Calu-6 cells, a well-known human renin-producing cell model.

Firstly, we employed a knockdown approach to suppress the expression of RRBP1 in the Calu-6 cells. This enabled us to study the impact of RRBP1 on renin expression. Figure 12A represents the results of this knockdown experiment.

Next, we sought to characterize the effect of RRBP1 on the distribution of renin. We examined the expression of renin within the RRBP1 knockdown (RRBP1-KD) cells and also measured the levels of renin released into the cultured media. Figure 12B illustrates the detection of renin expression within the RRBP1-KD cells, while Figure 12C depicts the levels of renin in the cultured media.

Remarkably, our findings revealed interesting patterns. In RRBP1-KD cells, the expression of renin was higher compared to non-knockdown cells. However, the level of renin released into the cultured media from RRBP1-KD cells was lower. This discrepancy suggests that RRBP1 may play a role in the distribution of renin within the cells and its subsequent release into the media.

By investigating renin expression in both RRBP1-KD cells and their cultured media, we have provided evidence for the involvement of RRBP1 in the regulation of renin. These results contribute to a deeper understanding of the mechanisms underlying renin production and secretion, shedding light on the role of RRBP1 in this process.
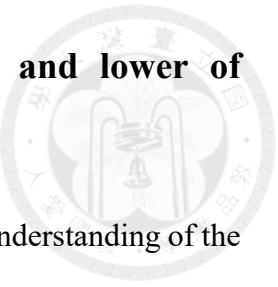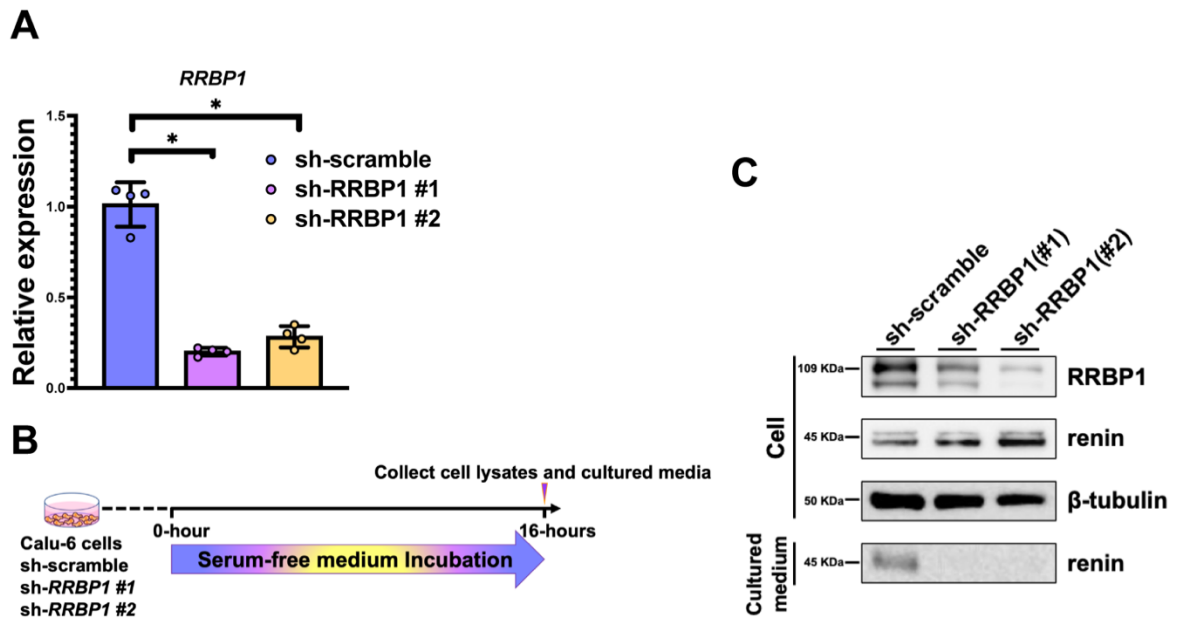
Figure 12. Renin distribution of *RRBP1*-KD cells. (**A**) The transcript level of *RRBP1* of scramble and sh-*RRBP1*-KD of Calu-6 cells were detected by quantitative RT-PCR (qRT-PCR). (**B**) experimental protocol of collecting cell lysates and cultured media of control and *RRBP1*-KD Calu-6 cells. (**C**) Renin expression in cell lysates and cultured media of control and *RRBP1*-KD Calu-6 cells. Lane 1 represents control cells. Lanes 2-3 represent *RRBP1*-KD cells. Data in (**A**) were measured by the 2 - ΔΔCt method with GAPDH as the reference gene (n=4 per group).

2-15 There were less renin particles near plasma membrane of *RRBP1*-KD cells.

In our ongoing investigation of RRBP1's role in renin distribution within renin-producing cells, we conducted additional experiments to gain further insights. Specifically, we utilized immunogold labeling and transmission electron microscopy (TEM) to examine the intracellular localization of renin in *RRBP1* knockdown (*RRBP1*-KD) cells.

To visualize and compare the distribution of renin, we performed immunogold labeling on the *RRBP1*-KD cells and a control group (scramble control cells). The labeled cells were then examined under a transmission electron microscope. Figures 13A to 13D present representative images obtained from this analysis.

Upon analyzing the collected data, we made several noteworthy observations. First, we discovered that there was a greater total number of intracellular particles in the *RRBP1*-KD cells compared to the control cells. This increase in total intracellular particles was found to be statistically significant (P-value<0.05), as depicted in Figure 13E.

Furthermore, we specifically assessed the distribution of renin particles located at a considerable distance from the plasma membrane (greater than 1000 nm). Surprisingly, the *RRBP1*-KD cells exhibited a higher number of these distant renin particles compared to the control cells (Figure 13F).

These findings suggest that in *RRBP1*-KD cells, there is an accumulation of renin particles within the cells rather than their secretion. The increased total number of intracellular particles, along with the higher proportion of distant renin particles, supports this notion.

By utilizing immunogold labeling and TEM, we have provided evidence of altered

renin distribution within *RRBP1*-KD cells. This contributes to our understanding of the role of RRBP1 in regulating the intracellular localization and secretion of renin in renin-producing cells.
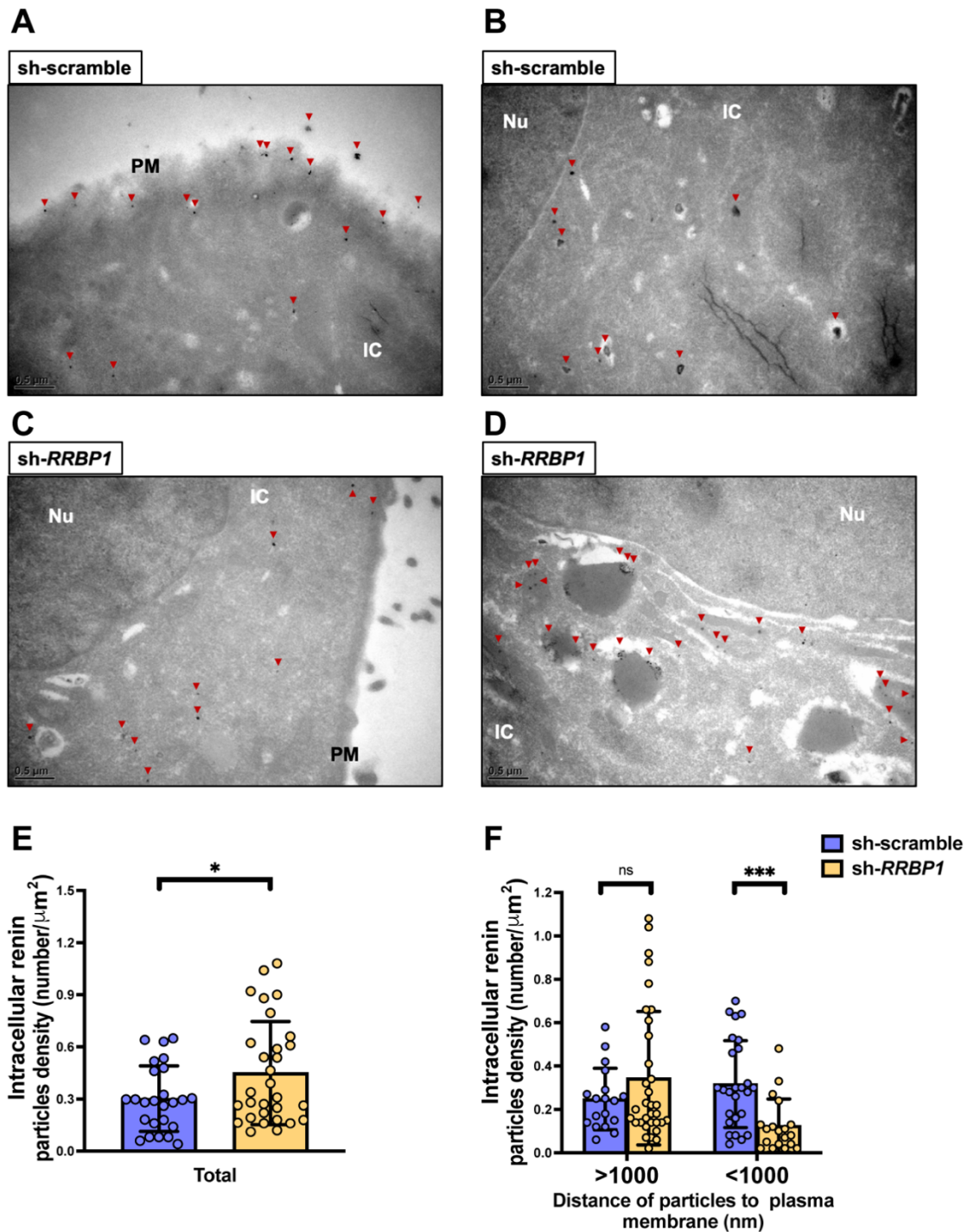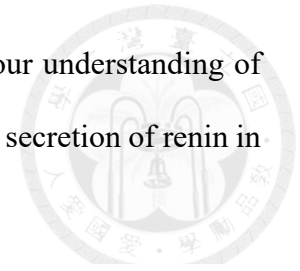
Figure 13. The immunogold-labeled renin staining by transmission electron microscopy. (**A**)-(**D**) transmission electron microscopy scanning image of

immunogold staining of Renin in control and *RRBP1*-KD Calu-6 cells. Dark red arrow indicates the nanogold particle (Scale bar= 0.5 μm). Nu, nucleus; IC, intracellular; PM, plasma membrane. (**E**) Quantification of total intracellular renin particles (**F**) Quantification of intracellular renin particles with distance more and less than 1000 nm from plasma membranes
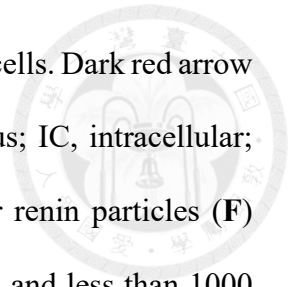
2-16 RRBP1 regulated renin secretion is in a cAMP-independent pathway.

In our study, we aimed to investigate the involvement of cyclic adenosine monophosphate (cAMP) in the regulation of renin secretion, as it is known to be a key regulator responsive to various external stimuli [41,90].

Initially, we assessed the transcript level of adenylyl cyclase 6 (*ADCY6*), which is the enzyme responsible for cAMP production [41,90]. Surprisingly, we found no significant difference in the transcript level of *ADCY6* between the control cells and *RRBP1* knockdown (*RRBP1*-KD) Calu-6 cells, as depicted in Figure 14A.

To further explore the role of cAMP in the context of RRBP1 deficiency, we treated the cells with forskolin, an activator of adenylyl cyclase known to elevate intracellular cAMP levels [41,90]. Our goal was to determine whether increasing cAMP levels could mitigate the effects of RRBP1 deficiency on renin production and secretion. Figure 14B represents the experimental setup.

Following forskolin treatment, we observed a significant increase in intracellular cAMP levels in both the control cells and *RRBP1*-KD cells, as demonstrated in Figure 14C. This indicated that forskolin effectively elevated cAMP levels in the cells, regardless of RRBP1 status.

Furthermore, we investigated the impact of forskolin treatment on renin production and secretion. Interestingly, forskolin treatment ameliorated the accumulation of intracellular renin in both the control and *RRBP1*-KD cells. However, there remained a lower level of renin secretion in the culture media of *RRBP1*-KD cells compared to the control cells (Figure 14D).

These results led us to conclude that RRBP1-regulated renin secretion occurs through a cAMP-independent pathway. Despite forskolin treatment increasing intracellular
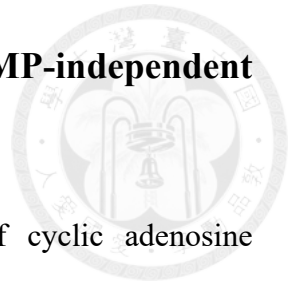
cAMP levels and partially improving the accumulation of intracellular renin in *RRBP1*-KD cells, the deficiency of RRBP1 still resulted in reduced renin secretion. Therefore, our findings suggest the involvement of alternative mechanisms and pathways, beyond cAMP regulation, through which RRBP1 influences renin production and secretion in renin-producing cells.
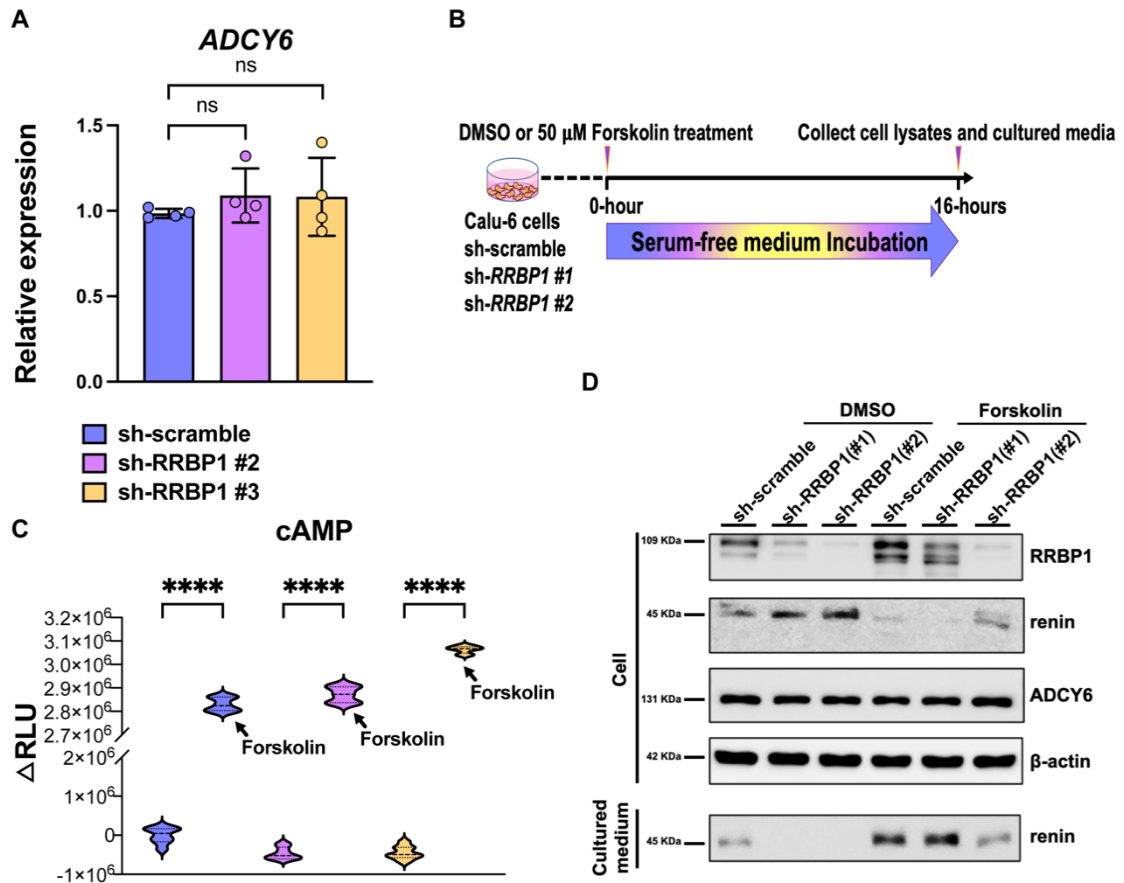
Figure 14. Forskolin treatment on control and *RRBP1*-KD Calu-6 cells. (**A**) The transcript levels of *ADCY6* in control and *RRBP1*-KD cells were analysis by quantitative RT-PCR. Data were measured using the 2 -ΔΔCt method with GAPDH as the reference gene. (n=4 per group) (**B**) Experimental protocol of forskolin stimulated renin production and secretion in control and *RRBP1*-KD cells. (**C**) The level of intracellular cAMP in control and *RRBP1*-KD cells with or without 50 μM forskolin treatment. Each bar represents the mean ±SEM. n=8 per group. Data in (**C**) were analyzed with Student unpaired 2-tailed t test.   Data were represented as mean

± SEM. ****P-value<0.0001 (**D**) The protein expression of RRBP1, renin, ADCY6 in control and *RRBP1*-KD cells with or without forskolin treatment. Lane 1 represents control cells and lanes 2-3 represent *RRBP1*-KD cells with DMSO control treatment. Lane 4 represents control cells and lanes 5-6 represent *RRBP1*-KD cells with 50 μM forskolin treatment.

2-17 Deficiency of RRBP1 results in accumulation of renin in endoplasmic reticulum.

To gain further insights into the dynamic intracellular trafficking of renin in control and *RRBP1* knockdown (*RRBP1*-KD) cells, we conducted fluorescence microscopy experiments using immunofluorescence-labeled renin, along with markers for the endoplasmic reticulum (calnexin) and Golgi apparatus (GOLIM4). These experiments were performed after forskolin induction, which is known to activate renin production and secretion.

Using confocal microscopy, we examined the distribution of renin in both control and *RRBP1*-KD cells at various time points (0, 60, 120, and 180 minutes) following forskolin treatment. Figure 15A provides an overview of the experimental setup.

Remarkably, our observations revealed distinct patterns of renin distribution between the control and *RRBP1*-KD cells over time. In the *RRBP1*-KD cells, renin appeared to be retained in the endoplasmic reticulum, even after 60, 120, and 180 minutes of forskolin treatment (Figure 15B-15E). In contrast, renin distribution in the control cells did not exhibit such significant retention in the endoplasmic reticulum.

To quantify and compare the fluorescence signal intensity of renin overlapping with calnexin (representing the endoplasmic reticulum), we performed an analysis. Surprisingly, there was no significant difference in the overlapped signal between the control and *RRBP1*-KD cells after 60 minutes of forskolin treatment. However, after 120 and 180 minutes of treatment, the *RRBP1*-KD cells exhibited a stronger overlapped fluorescent signal compared to the control cells (Figure 15F).

Conversely, we examined the overlapped fluorescent signal between renin and GOLIM4 (representing the Golgi apparatus). Interestingly, the *RRBP1*-KD cells showed a weaker overlapped fluorescent signal of renin and GOLIM4 compared to

the control cells at all time points (0, 60, 120, and 180 minutes) following forskolin treatment (Figure 15G-15K). We also stain RRBP1 in Figure 15L-15O.

Taken together, our fluorescence microscopy results provide evidence of altered intracellular trafficking of renin in *RRBP1*-KD cells. The retention of renin in the endoplasmic reticulum and reduced association with the Golgi apparatus suggests impaired trafficking and secretion of renin in the absence of RRBP1. These findings deepen our understanding of the role of RRBP1 in the intracellular transport of renin within renin-producing cells.

A

sh-scramble

sh-*RRBP1*

B 0 min

C 60 min

D 120 min

E 180 min

F

Calnexin-Renin Overlap Coefficient

Forskolin incubation time (mins)

sh-scramble
sh-*RRBP1*
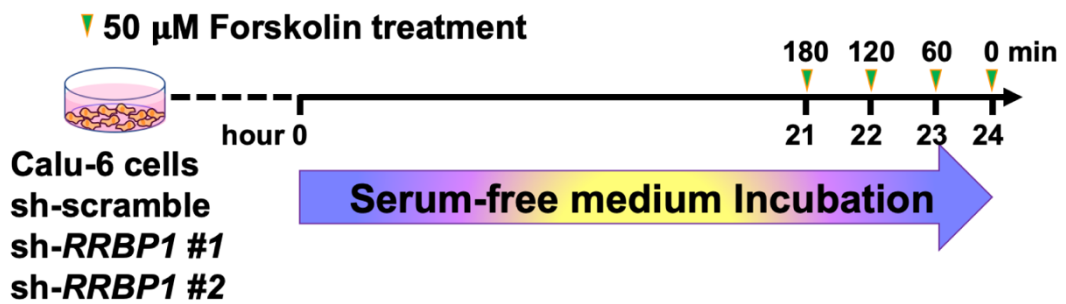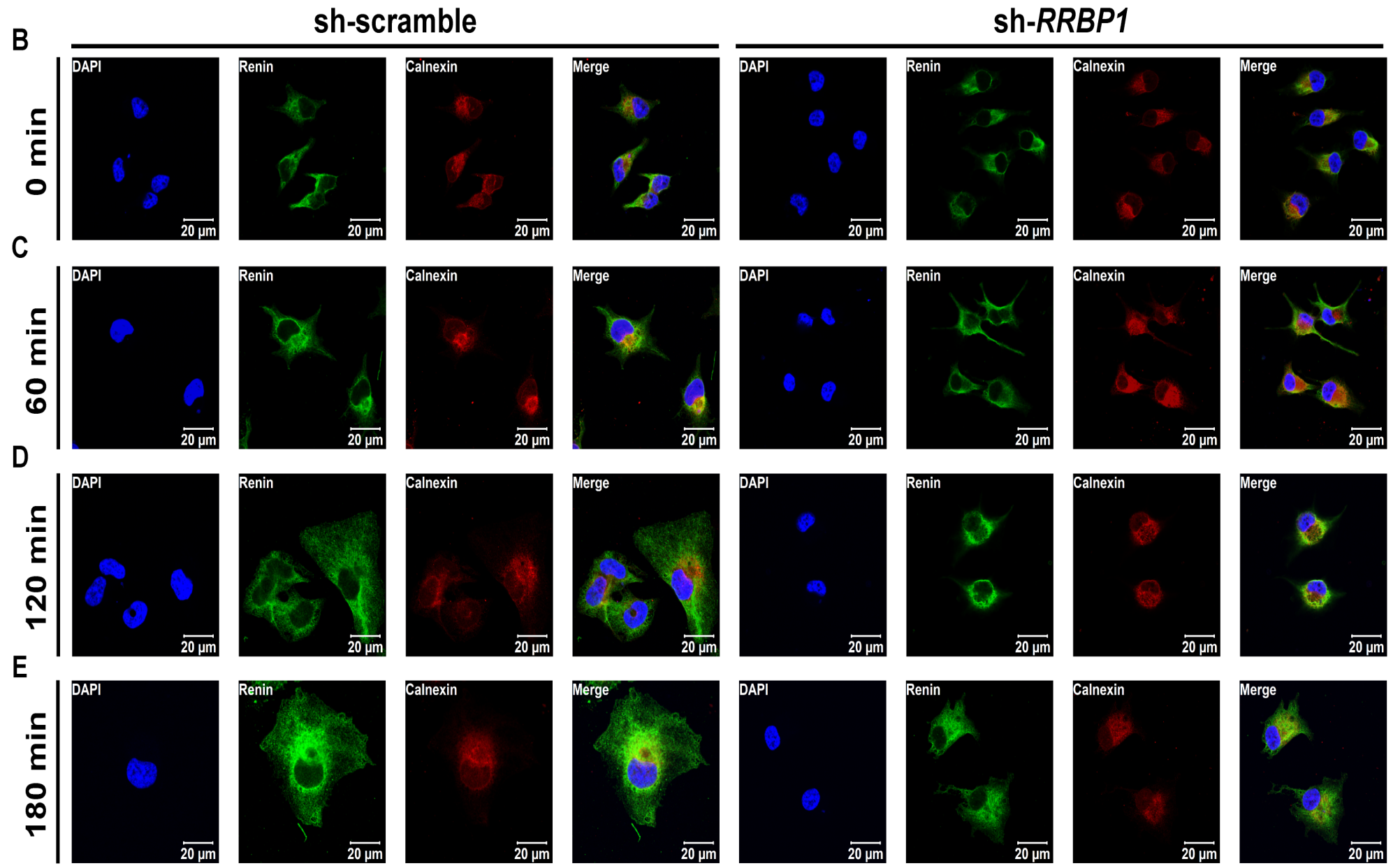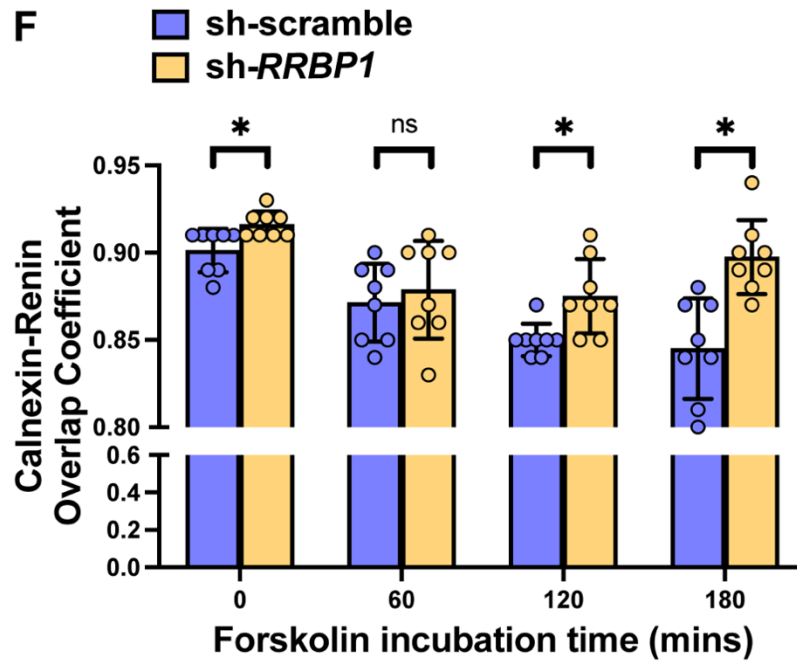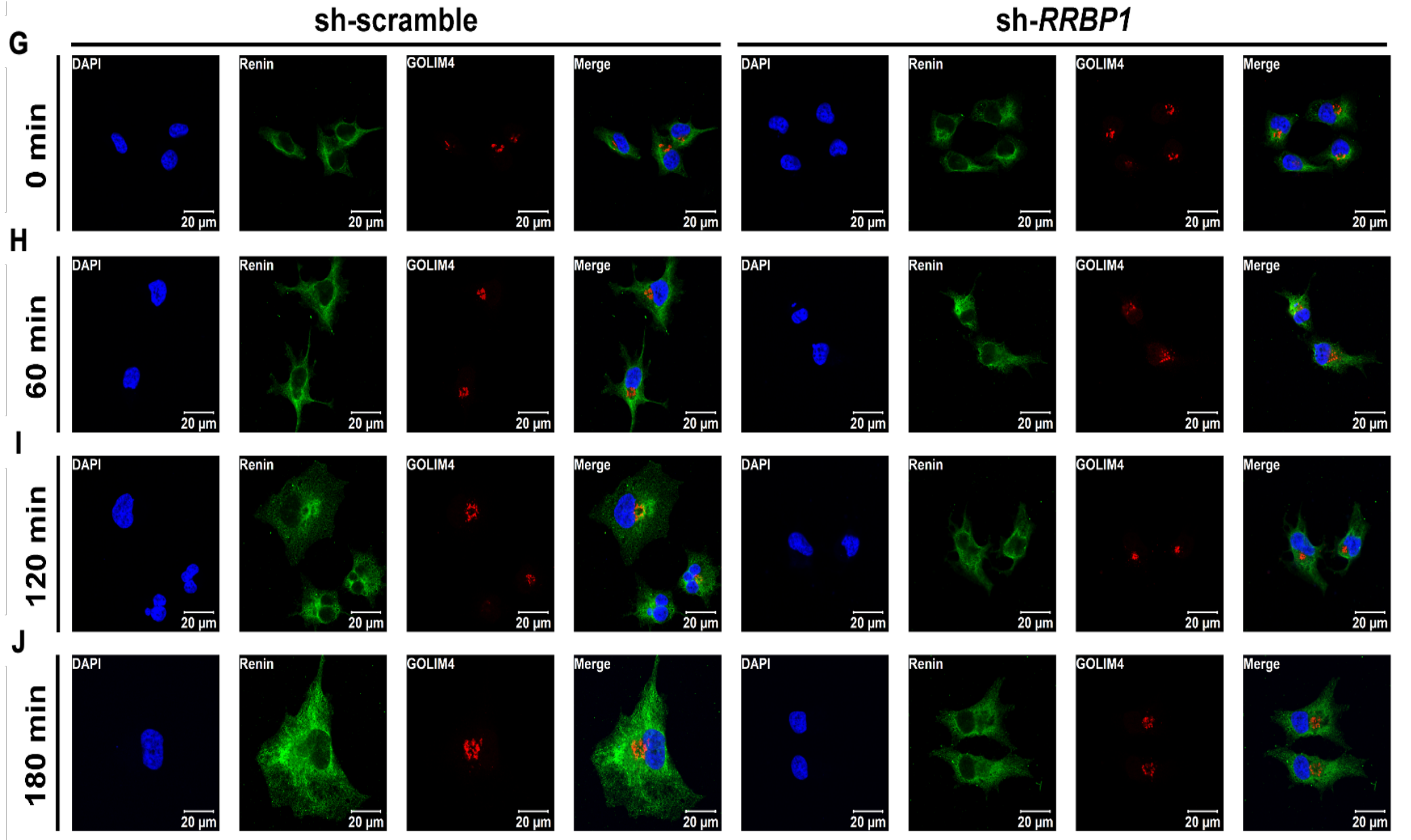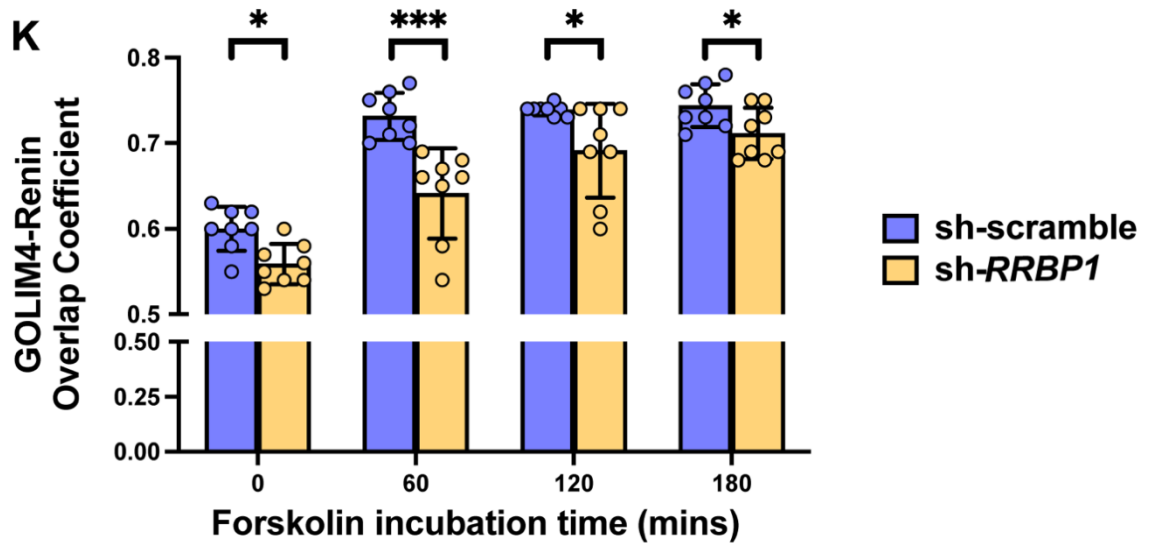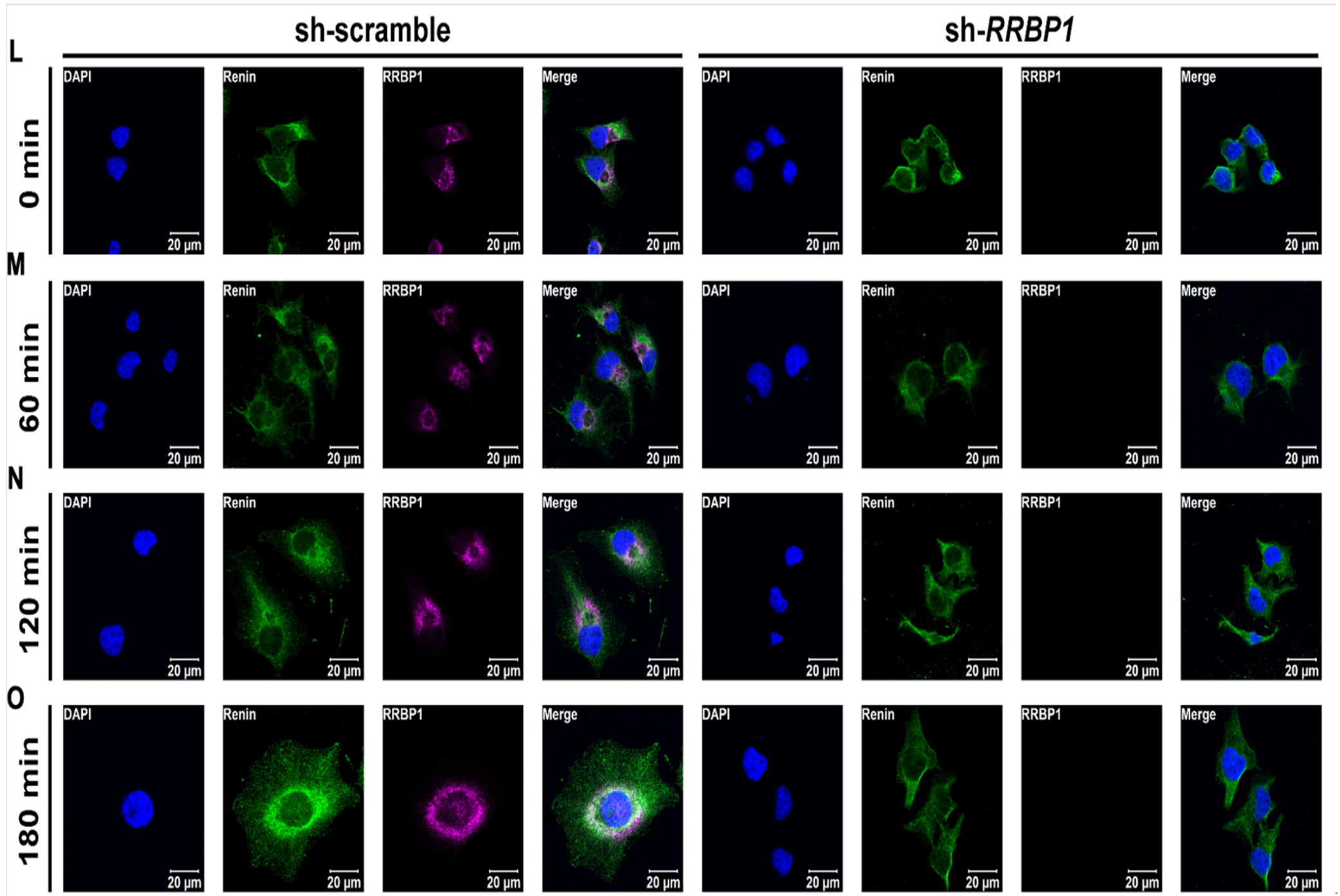
Figure 15. Intracellular renin trafficking in *RRBP1*-KD cells. (**A**) Experimental protocol of forskolin induced renin trafficking in control and *RRBP1*-KD cells. (**B**)-(**E**) Immunofluorescent images of control and *RRBP1*-KD cells after 50 µM forskolin treatment for 0, 60, 120, and 180 minutes by confocal microscopy. Renin (green), Calnexin (red), and DAPI (blue) (**F**) The overlap coefficients of Renin (green) and Calnexin (red) in control and *RRBP1*-KD Calu-6 cells (n=8 per group) (**G**)-(**J**) Immunofluorescent images of control and *RRBP1*-KD cells after 50 µM forskolin treatment for 0, 60, 120, and 180 minutes by confocal microscopy. Renin (green), GOLIM4 (red), and DAPI (blue) (**K**) The overlap coefficients of Renin (green) and GOLIM4 (red) in control and *RRBP1*-KD Calu-6 cells (n=8 per group) Data in (**F**) and (**K**) were analyzed with Student unpaired 2-tailed t test. Data were represented as mean ± SEM. * P-value<0.05; *** P-value<0.001 (**L**)-(**O**) Immunofluorescent images of control and *RRBP1*-KD cells after 50 µM forskolin treatment for 0, 60, 120, and 180 minutes by confocal microscopy. Renin (green), RRBP1 (red), and DAPI (blue)

2-18 Deficiency of RRBP1 lead to hyporeninemic hypoaldosteronism, hypotension, and hyperkalemia

In summary, our comprehensive findings highlight the crucial role of RRBP1 in the intracellular trafficking of renin, specifically from the endoplasmic reticulum to the Golgi apparatus, as well as in renin secretion. The loss of RRBP1 leads to several significant consequences, including hyporeninemic hypoaldosteronism, hypotension, and hyperkalemia (Figure 16).

Our research demonstrates that RRBP1 deficiency affects renin distribution and secretion in renin-producing cells. Through various experimental approaches, we have shown that *RRBP1* knockdown results in the retention of renin within the endoplasmic reticulum, impaired association with the Golgi apparatus, and reduced renin secretion.

These alterations in renin trafficking and secretion have important physiological implications. The observed hyporeninemic hypoaldosteronism suggests a decreased production of renin, which in turn leads to reduced aldosterone synthesis. Consequently, this hormonal imbalance contributes to hypotension, a decrease in blood pressure. Additionally, the impaired renin secretion contributes to hyperkalemia, an elevation in blood potassium levels.

Collectively, our findings highlight the essential role of RRBP1 in the regulation of renin trafficking and secretion, as well as its impact on physiological processes such as blood pressure and electrolyte balance. Understanding the mechanisms underlying these effects provides valuable insights into the intricate pathways involved in renin production and secretion, with potential implications for the management of conditions associated with renin dysregulation.
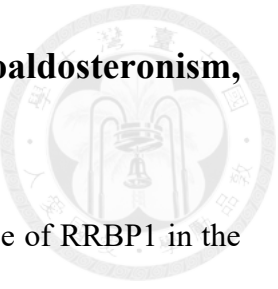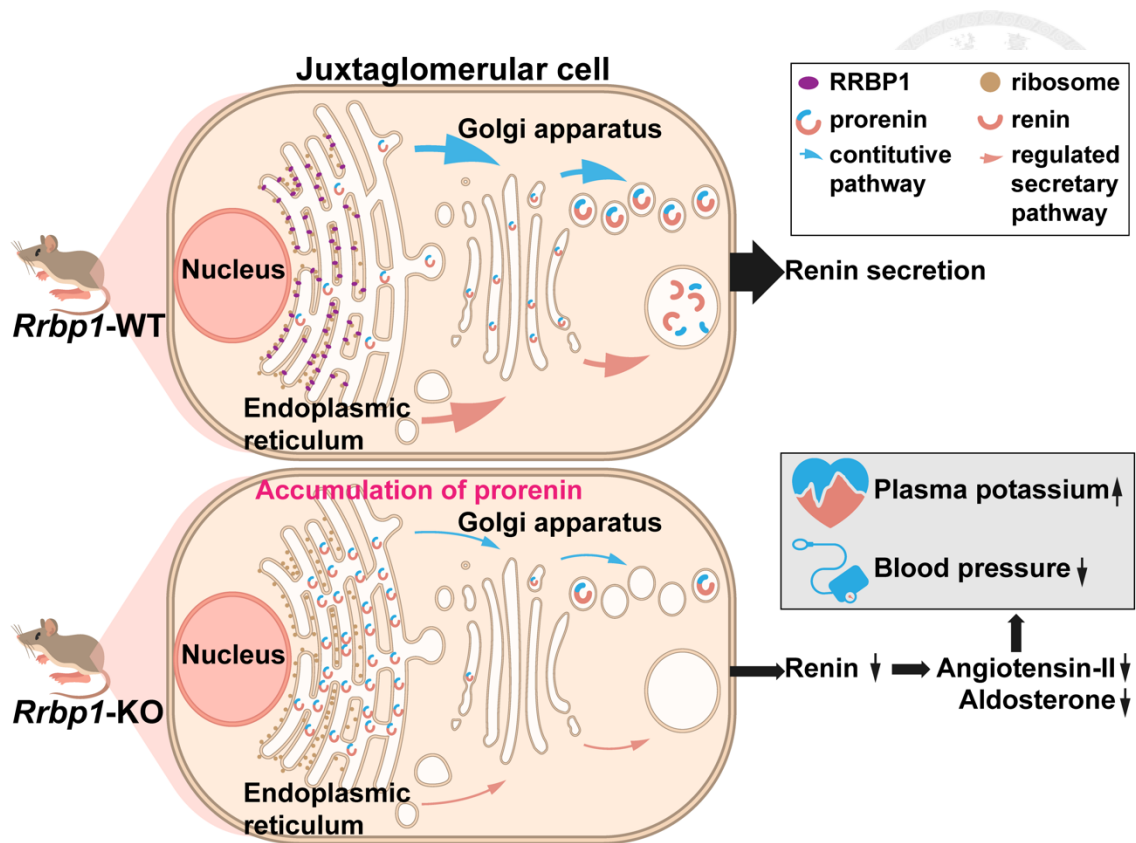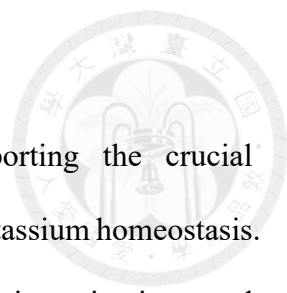
Figure 16. Schematic diagram of the mechanism by which RRBP1 affects renin trafficking and secretion.
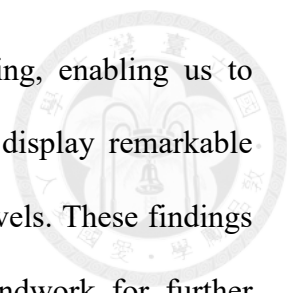
3. Discussion

Our research findings have yielded robust evidence supporting the crucial involvement of RRBP1 in the regulation of blood pressure and potassium homeostasis. By employing a multifaceted approach encompassing genetic investigations and animal model experiments, we have successfully elucidated a significant correlation between RRBP1 and the modulation of blood pressure. Through our comprehensive analysis of the SAPPHIRe cohort, which included family-based genome-wide linkage studies and regional fine mapping, we identified specific genetic variants within the RRBP1 gene that exhibit strong associations with systolic, diastolic, and mean blood pressure levels [113].

The culmination of our investigation provides compelling insights into the pivotal role of RRBP1 in maintaining blood pressure and potassium balance within the body. Through meticulous genetic analysis techniques and rigorous animal model experiments, we have not only established a substantial connection between RRBP1 and blood pressure regulation but also shed light on the underlying mechanisms involved. Leveraging the diverse range of data obtained from our family-based genome-wide linkage analysis, we successfully pinpointed distinct genetic variants located within the RRBP1 gene that demonstrate significant correlations with systolic, diastolic, and mean blood pressure measurements. This discovery reinforces the importance of RRBP1 as a key player in the intricate network of pathways governing blood pressure regulation [113].

Our comprehensive approach, integrating genetic investigations and animal model studies, has provided a comprehensive framework for understanding the significance of RRBP1 in blood pressure and potassium homeostasis regulation. Through rigorous examination of the SAPPHIRe cohort, we meticulously conducted family-based

genome-wide linkage analyses and region-specific fine mapping, enabling us to identify specific genetic variants residing within RRBP1 that display remarkable associations with systolic, diastolic, and mean blood pressure levels. These findings contribute valuable knowledge to the field and lay the groundwork for further exploration of the intricate interplay between RRBP1 and blood pressure regulation [113].

In summary, our research findings underscore the crucial role of RRBP1 in the intricate orchestration of blood pressure regulation and potassium homeostasis. Our extensive investigations, incorporating genetic and animal model studies, have successfully elucidated the profound impact of RRBP1 on blood pressure control [113]. By leveraging advanced genetic analysis techniques and thorough examination of the SAPPHIRe cohort, we have identified specific genetic variants within the RRBP1 gene that exhibit robust associations with systolic, diastolic, and mean blood pressure measurements. These significant findings pave the way for future studies aimed at unraveling the intricate molecular mechanisms underlying blood pressure regulation, ultimately leading to the development of novel therapeutic interventions [113].

To further investigate the functional implications of RRBP1, we conducted studies using mouse models. The deficiency of RRBP1 in mice resulted in lower blood pressure, severe hyperkalemia, and sudden arrhythmic death. These mice exhibited hyporeninemic hypoaldosteronism, a condition characterized by reduced renin levels and impaired aldosterone synthesis. However, treatment with fludrocortisone, a synthetic mineralocorticoid, was able to rescue the typical features of hyporeninemic hypoaldosteronism in these mice [113].

Our investigation into the cellular mechanisms revealed that RRBP1 deficiency leads

to the accumulation of renin within the endoplasmic reticulum, resulting in decreased renin secretion. Immunofluorescence imaging and electron microscopy analysis confirmed the retention of renin in the endoplasmic reticulum and reduced transport to the Golgi apparatus in RRBP1-deficient cells [113].

In addition to its role in blood pressure regulation, RRBP1 has been implicated in various cardiac vascular diseases, including intracranial arterial aneurysm and coronary artery diseases. Genetic studies have also identified associations between RRBP1 variants and lipoprotein levels. Furthermore, functional studies have demonstrated the involvement of RRBP1 in the modulation of lipid synthesis and ER-mitochondria contacts, which impact VLDL synthesis.

The physiological consequences of RRBP1 deficiency in mice were consistent with our observations in humans. *Rrbp1*-knockout mice displayed lower blood pressure, increased susceptibility to sudden death, and abnormal electrocardiogram patterns indicative of hyperkalemia. These findings suggest that severe hyperkalemia is a major contributor to the sudden death observed in *Rrbp1*-knockout mice. Fludrocortisone treatment improved survival rates by addressing the hyperkalemia and associated renal tubular potassium excretion defect [113].

Notably, despite the accumulation of renin within the kidney tissue of *Rrbp1*-knockout mice, there was a lower level of renin in the circulation, indicating impaired secretion from juxtaglomerular (JG) cells, the primary producers of renin. This discrepancy highlights the importance of RRBP1 in the intracellular trafficking and secretion of renin [113].

Furthermore, our investigations into renin production using the Calu-6 cell line, a renin-producing cell model, revealed that RRBP1 deficiency led to increased intracellular renin levels but reduced renin secretion. Transmission electron
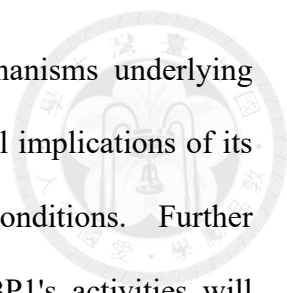
microscopy images further demonstrated the accumulation of renin within the endoplasmic reticulum and decreased localization near the plasma membrane in RRBP1-deficient cells [113].

RRBP1, an essential ribosomal binding protein, resides in the membranes of the endoplasmic reticulum (ER). Its pivotal function lies in facilitating the association between ribosomes and transcripts that encode proteins intended for the secretory pathway. By establishing this crucial connection, RRBP1 plays a vital role in the proper processing and transportation of proteins within the cell. Moreover, this multifaceted protein exerts its influence on ER morphology by binding to microtubules, thereby influencing protein trafficking and secretion processes [113].

The involvement of RRBP1 in various cellular processes has been well-documented. Its deficiency has been shown to have significant implications on the synthesis and secretion of important biomolecules. For instance, studies have revealed that the absence or reduced expression of RRBP1 leads to disruptions in the production and release of apolipoproteins, which are crucial components of lipoprotein particles involved in lipid metabolism. This deficiency also impairs the synthesis and secretion of collagen, a major structural protein that provides strength and support to various tissues in the body. Additionally, the absence of RRBP1 has been linked to abnormalities in very low-density lipoprotein (VLDL) synthesis and secretion, contributing to disruptions in lipid transport and metabolism.

Through its pivotal role in the association of ribosomes with transcripts and its impact on ER morphology, RRBP1 serves as a key regulator of protein synthesis, processing, and secretion. Its deficiency disrupts the finely tuned balance of these cellular processes, leading to impaired production and secretion of crucial biomolecules like apolipoproteins, collagen, and VLDL. Understanding the intricate functions of
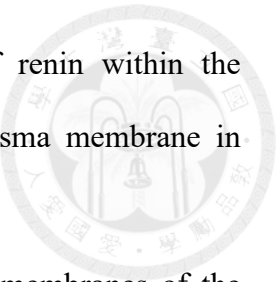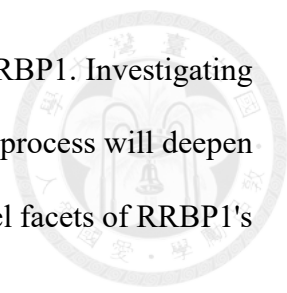
RRBP1 provides valuable insights into the fundamental mechanisms underlying protein trafficking and secretion, and sheds light on the potential implications of its deficiency in various physiological and pathological conditions. Further investigations into the molecular mechanisms governing RRBP1's activities will deepen our understanding of its biological significance and may uncover new avenues for therapeutic interventions targeting protein synthesis and secretion disorders.

While our study has yielded valuable insights into the involvement of RRBP1 in renin regulation and blood pressure control, there remain intriguing questions that warrant further investigation. Future research endeavors should aim to unravel the contribution of additional tissues and organs in the complex regulation of blood pressure, considering that RRBP1 exhibits universal expression rather than exclusive localization in juxtaglomerular (JG) cells. The exploration of these aspects will provide a more comprehensive understanding of the multifaceted role of RRBP1 in maintaining blood pressure homeostasis [113].

To delve deeper into the phenotypic effects of RRBP1 deficiency, it would be beneficial to utilize cell- or tissue-specific knockout mouse models. By selectively targeting RRBP1 in specific cell types or tissues, researchers can assess the specific impact of its deficiency on blood pressure regulation and related physiological processes. These models will offer valuable insights into the distinct roles of RRBP1 in various cellular contexts, enabling a more nuanced understanding of its contributions to overall blood pressure control [113].

Furthermore, the precise mechanisms through which RRBP1 regulates protein trafficking from the endoplasmic reticulum (ER) to the Golgi apparatus remain incompletely defined. While RRBP1's role in facilitating ribosome association and its influence on ER morphology are known, there may be additional molecular players

involved in the intricate protein trafficking process elicited by RRBP1. Investigating the potential involvement of other molecules or pathways in this process will deepen our understanding of the underlying mechanisms and unveil novel facets of RRBP1's function [113].

By addressing these outstanding questions, future studies can enhance our comprehension of the broader regulatory network governing blood pressure and shed light on the specific roles and molecular interactions of RRBP1. This expanded knowledge may have implications for the development of targeted therapeutic approaches aimed at manipulating RRBP1 or its associated pathways for the management of blood pressure disorders and related conditions [113].

In summary, our research establishes RRBP1 as a novel and important regulator of renin trafficking, intracellular protein secretion, and blood pressure. The findings from our studies in humans and mice support the potential use of *Rrbp1*-knockout mice as a valuable model for investigating the regulation of renin synthesis and secretion, as well as the pathogenesis of hyporeninemic hypoaldosteronism. Moreover, the identification of RRBP1 as a regulator of blood pressure and potassium homeostasis offers new avenues for understanding and potentially targeting these physiological processes in various cardiovascular and renal disorders [113].

4. Material and methods
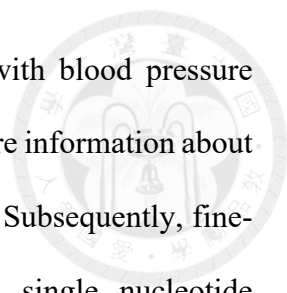
4-1 The Stanford Asia-Pacific Program for Hypertension and Insulin Resistance (SAPPHIRe) cohort

The Stanford Asia-Pacific Program for Hypertension and Insulin Resistance (SAPPHIRe) is a collaborative family study funded by the Family Blood Pressure Program of the National Heart, Lung, and Blood Institute. This study aimed to identify the genetic factors underlying hypertension and insulin resistance in individuals of Chinese ancestry. The cohort consisted of over 1,144 participants, including sibling pairs who were either concordant or discordant for high blood pressure. Detailed information about the study cohort can be found in our previous publication [91]. High blood pressure was defined as systolic blood pressure >140 mm Hg and diastolic blood pressure >90 mm Hg or the use of two hypertension medications. Low-normal blood pressure was defined as blood pressure in the bottom 30% of the age- and sex-adjusted distribution. Participants with heart, liver, kidney diseases, or chronic conditions such as diabetes or cancer were excluded from the study. The study protocol was approved by the Institutional Review Boards/Research Ethics Review Committees, including those at National Taiwan University Hospital, National Health Research Institutes, Taichung Veterans General Hospital, Taipei Veterans General Hospital, and Tri-Service General Hospital. All participants provided informed consent, and the study followed the principles outlined in the Declaration of Helsinki. Further details of the analysis can be found in the Supplementary information online.

4-2 Genome-wide linkage and family-based association analyses for identification of blood pressure regulation genes

Initially, genome-wide linkage analysis was conducted on the SAPPHIRe cohort, which included 1,144 subjects of Chinese origin from 360 nuclear families. This

analysis revealed a quantitative trait locus (QTL) associated with blood pressure variations located on chromosome 20 between 14.7-18.3 Mb. More information about the linkage analysis can be found in our previous work [91, 92]. Subsequently, fine-mapping was performed within this QTL region using 51 single nucleotide polymorphisms (SNPs) in six genes: PCSK2, BFSP1, RRBP1, SNX5, OVOL2, and CSRP2BP. Family-based association tests (FBAT) were applied to analyze single-SNP and SNP-haplotype associations [92]. Sliding window approaches were used to identify haplotypes associated with blood pressure. Haplotype analyses and permutation procedures were performed using the "hbat" module in FBAT.

4-3 Generation of Rrbp1-knockout mice

To generate Rrbp1-knockout mice, we employed the recombineering-based method and created two targeting vectors. The purpose was to delete exons 4-24 of the Rrbp1 gene [93]. First, LoxP sites were inserted upstream of exon 4 and downstream of exon 24 within the Rrbp1 gene using DNA fragments retrieved from the 129/Sv-derived bacterial artificial chromosome clones. These DNA fragments were separately inserted into a retrieving vector, PL253, which includes a thymidine kinase cassette for negative selection of embryonic stem (ES) cells. The vectors were designed to insert a neomycin resistance cassette flanked by LoxP sites upstream of exon 4 and a neomycin cassette flanked by Frt sites and a LoxP site downstream of exon 24.

The first targeting vector, targeting exon 4, was linearized and introduced into 129/Sv-derived ES cells (R1) through electroporation. Correctly targeted clones were confirmed using Southern blotting, and the neomycin resistance gene was removed through the expression of Cre recombinase. Subsequently, the second targeting vector, targeting exon 24, was introduced into the resulting ES cells, followed by confirmation using Southern blotting. After the deletion of the Rrbp1 gene mediated

by Cre, the selected ES cells were injected into C57BL/6 blastocysts to generate chimeric mice. The male chimeras were crossed into a C57BL/6 background to establish the Rrbp1-knockout mouse line.

For genotyping, genomic DNA was extracted from mouse tails, and PCR amplification was performed using specific primer sets. The wild-type primer set amplified the region with forward primer 5'- AGAGAATGGTTGGGATAGAG -3' and reverse primer 5'- CAAACCCTTGTCATGAGCAT -3'. The knockout primer set amplified the region with forward primer 5'- CACTACATGTGTAGCTGAAC -3' and reverse primer 5'- CAAACCCTTGTCATGAGCAT -3'.

To conduct a high-potassium loading mouse survival test, mice were subjected to a high potassium intake regimen and received intraperitoneal injections of fludrocortisone acetate every two days for a total of 30 days. The occurrences of death were recorded. For tissue analysis or euthanasia, mice were sacrificed following the guidelines of the Institutional Animal Care and Utilization Committee and in accordance with the National Institutes of Health (NIH) guidelines for the Care and Use of Laboratory Animals.

4-4 Western blot analysis

To perform Western blot analysis, mouse tissues and cell lysates were extracted using RIPA lysis buffer (Millipore, 20-188) following the manufacturer's protocol. Culture medium from cells was collected and concentrated using Amicon Ultra-15 tubes (Millipore, 10 KDa). The following antibodies were used for detection: anti-RRBP1 (Invitrogen, PA5-21392; Abcam, Ab95983; Sigma, HPA011924), anti-Hsp70 (Affinity, DF2698), anti-β-actin (Genetex, GTX109697), anti-renin (Abnova, H0005972-M01), anti-ACE (Invitrogen, MA5-32741), anti-β-tubulin (Taiclone, tcaba2), anti-SGK1 (Abcam, ab32374), anti-ADCY5/6 (Abnova, PA5-75274), and

anti-calnexin (Abcam, ab22595). The blots were visualized using Trident pico Western HRP Substrate solution (Genetex, GTX17435) and analyzed using a UVP BioSpectrum Auto Imaging System.
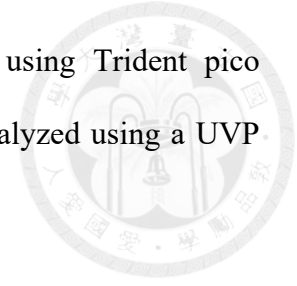
4-5 Body composition analysis

The body compositions of 16-week-old mice were determined using the SkyScan1076 high-resolution micro-CT system. Mice were anesthetized with 1% isoflurane inhalation. We acknowledge the technical support in standard body composition analysis provided by the Taiwan Mouse Clinic, Academia Sinica, and Taiwan Animal Consortium.

4-6 Intracranial vessel scanning by magnetic resonance angiography

All imaging was conducted using a 7-T scanner (PharmaScan 70/16, Bruker Biospin GmbH, Germany) equipped with an actively shielded gradient capable of producing a maximum gradient amplitude of 300 mT/m with an 80 μs. The mice were initially anesthetized with 5% isoflurane in air at a flow rate of 1 L/min. Once fully anesthetized, the mice were placed in a prone position and positioned with a custom-designed head holder inside the magnet. Anesthesia was maintained with 1.0-1.2% isoflurane in air at a flow rate of 1 L/min throughout the experiments. Images were acquired using a 38-mm birdcage transmitter coil and a separate quadrature surface coil for signal detection.

To determine 3-dimensional $\Delta R2$ micro magnetic resonance angiography (3D$\Delta R2$-μMRA), T2-weighted images (T2WIs) were acquired before and after the injection of superparamagnetic iron oxide nanoparticles at a dose of 20 mg/kg. The acquisition of post-contrast images was delayed by 1-2 minutes to ensure that the distribution of the contrast agent in the vascular network reached a steady state. T2WIs were obtained using a 3D fast spin echo (FSE) sequence with the following parameters: repetition

time of 1,800 ms, effective echo time (TE) of 80 ms, 2 averages, a field of view of 2.0 × 2.0 × 1.0 cm, an acquisition matrix of 512 × 192 × 96, and a total acquisition time of 1 hour and 9 minutes.

4-7 Telemetry ECG and blood pressure measurements

For non-invasive ECG recording, 12-16-week-old mice were anesthetized with 2.5% isoflurane in pure oxygen at a flow rate of 0.5 L/min. Mouse ECGs were recorded and analyzed using Powerlab8/30 and Animal Bio Amp. Telemetry ECG recording was performed on the same age group of mice. They were anesthetized with 2.5% isoflurane in pure oxygen at a flow rate of 0.5 L/min. Telemetric transmitters (ETA-F10, Data Sciences International) were implanted in the neck with electrodes, as previously described [96], and tunneled subcutaneously. Two-hour ECG recordings were obtained from conscious mice before and during high potassium intake for 2 days. The recordings were analyzed using Dataquest A.R.T. Software (Data Sciences International).

To ensure adaptability and reduce stress during the measurements, mice weighing 25-30 g and aged 10-16 weeks were placed in plastic tube restrainers for over 10 minutes. This adaptive training step was performed daily for one week before recording. Each mouse underwent more than 60 measurements. Between 1:00 pm and 3:00 pm, systolic blood pressure (SBP), diastolic blood pressure (DBP), and mean blood pressure (MBP) were measured using a noninvasive tail-cuff blood pressure monitor (MOORLAB NIBP, MOOR).

4-8 Blood and urine analysis

Male and female mice aged 10-16 weeks were used for the following assays. For the high potassium loading test or fludrocortisone acetate treatment assay, mice were placed in metabolic cages at 11:00 am. They were initially fed a control diet

(D10012Mi, Research Diets) and normal water for 24 hours, followed by a high-K+ diet (5% potassium added as potassium chloride) and water containing 5% KCl for an additional 48 hours. In the fludrocortisone acetate treatment assay, mice received intraperitoneal injections of either saline or 100 mg/kg fludrocortisone acetate (F6127, Sigma) after 24 hours of high-K+ intake. After another 24 hours, urine and blood samples were collected from the submandibular vein for analysis.

The electrolyte profile was determined using different kits on a cobas c11 analyzer (Roche). Plasma samples with a hemolysis index ranging from zero to "++" (indicating a very mild level of hemolysis) were used for electrolyte measurement and ELISA assays. Commercial ELISA kits were used to measure the levels of renin (Elabscience, E-EL-M0061), angiotensinogen (Cusabio, CSB-E08566m), Ang-I (Cusabio, CSB-E08529m), Ang-II (Cusabio, CSB-E04495m), aldosterone (Enzo Life, ADI-900-173), and noradrenaline (Cusabio, CSB-E07870m). Renin activity was determined using the SensoLyte®520 Mouse Renin Assay Kit (AnaSpec, AS-72161). Ten µl of serum sample was used to measure mouse renin activity by monitoring the fragments of 5-FAM at excitation/emission = 490/520 nm using a 5-FAM/QXL™ 520 fluorescence resonance energy transfer peptide.

4-9 ACTH stimulation test

At 16 weeks of age, mice were intraperitoneally injected with Adrenocorticotropic Hormone (ACTH 1-24; A0928, Sigma) at a dose of 50 ng/g body weight at 11:00. Blood samples were collected at 0, 30, 60, and 90 minutes after ACTH treatment. The levels of corticosterone were measured using commercial ELISA kits (Cusabio, CSB-E07969m).

4-10 Real-time quantitative PCR (RT-qPCR)

RNA samples were extracted from the experimental samples using TRIzol® reagent

(Life Technologies). A total of 2 µg of total RNA was reverse transcribed into cDNA using a reverse transcriptase kit (HD life science). The RT-qPCR assay was performed on a LightCycler® 480 System Real-Time PCR System (Roche) using SYBR-Green qPCR mix (HD life science). The primer sequences used for amplification were as follows:

- RRBP1:

  - Forward: 5′-TACGACACTCAAACCTTGGGG-3′

  - Reverse: 5′-GGTTGGCTAGGGCTTCTTCATA-3′

- ADCY6:

  - Forward: 5′-GCTCATGGTGGTGTGTAACC-3′

  - Reverse: 5′-GCGTGTAGGCGATGTAGACAAA-3′

- Scnn1a:

  - Forward: 5′-CCTTCTCCTTGGATAGCCTGG-3′

  - Reverse: 5′-CAGACGGCCATCTTGAGTAGC-3′

- Scnn1b:

  - Forward: 5′-GGCCCAGGCTACACCTACA-3′

  - Reverse: 5′-AGCAGCGTAAGCAGGAACC-3′

- Scnn1g:

  - Forward: 5′-GCACCGACCATTAAGGACCTG-3′

  - Reverse: 5′-GCGTGAACGCAATCCACAAC-3′

- GAPDH:

  - Forward: 5′-CTGGGCTACACTGAGCACC-3′

  - Reverse: 5′-AAGTGGTCGTTGAGGGCAATG-3′

The amplification reactions were carried out according to the manufacturer's instructions, and the relative expression levels of the target genes were analyzed using the LightCycler® 480 System software.

4-11 Renal Immunohistochemistry

Mouse kidneys and adrenal glands were embedded in paraffin, and 4-µm tissue sections were cut from the paraffin blocks and placed on slides. Hematoxylin and eosin staining was performed on the adrenal gland sections as per standard protocol. For the kidney sections, the following steps were carried out:

1. The sections were rehydrated by sequential immersion in xylene, followed by 100%, 95%, 70%, and 50% alcohol solutions.

2. Antigen retrieval was performed by immersing the sections in a 1 mM Citrate acid buffer (pH 6.0) with tween 20 and heating them to 92-95 °C.

3. To block endogenous peroxidase activity, the sections were incubated in 3% H_2O_2 for 20 minutes.

4. Tissue blocking was performed using 3% BSA/PBST.

5. Immunohistochemistry staining was conducted using a primary antibody for renin (dilution: 1:20; H0005972-M01, Abnova), secondary antibodies HRP-anti-rabbit/mouse (K5007, Dako), and DAB chromogen solution.

6. The stained sections were digitized using an advanced microscope (Axio Imager. A1, Zeiss).
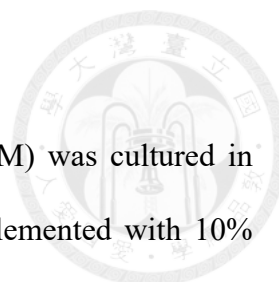
4-12 Calu-6 Cell Culture

The human renin-secreting Calu-6 cell line (ATCC, HTB-56TM) was cultured in Dulbecco's modified Eagle medium/nutrient mixture F12 supplemented with 10% fetal bovine serum (FBS) and 1% penicillin-streptomycin (p4333, Sigma). The cells were maintained at 37°C in a humidified incubator with 5% CO_2. Routine culturing was performed in 10-cm plastic tissue culture dishes (430167, Corning Inc.), and the cells were harvested with trypsin when they reached the logarithmic growth phase.

4-13 Lentiviral Transfection

Lentiviral knockdown particles targeting RRBP1 and lentiviral scramble control particles were obtained from the RNAi core at Academia Sinica, Taiwan. The following steps were performed for cell infection:

1. Calu-6 cells at 45-55% confluency were incubated with lentiviral particles and 24 μg polybrene in 3 ml of growth medium at a multiplicity of infection of 10.

2. After 24 hours, the medium was replaced with 4 ml of fresh growth medium.

3. After 48 hours, the medium was again replaced with 4 ml of fresh growth medium, supplemented with 8 μg puromycin (A1113802, Thermo Fisher) for cell selection.

4. After five days, all transfected Calu-6 cells were passaged for further experiments. The efficiency of RRBP1 knockdown was examined using qPCR and western blotting analyses.

4-14 Immuno-electron Microscopy

Calu-6 cells were plated on plastic coverslips in 60-mm tissue culture plates and incubated for two days. The following steps were carried out for immuno-electron microscopy:

1. Cells were fixed with a solution of 2% paraformaldehyde and 1% glutaraldehyde

in 0.1 M phosphate buffer (pH 7.4) for 40 minutes.

2. Samples were blocked and permeabilized with PBS containing 5% BSA and 0.1% saponin for 30 minutes.

3. Incubation with primary antibodies for renin (dilution: 1:20; H0005972-M01, Abnova) was performed in PBS containing 5% BSA and 0.05% saponin for 2 hours at room temperature.

4. After washing the samples with PBS four times, they were incubated with a secondary antibody (dilution: 1:100; 2002 Nanogold®-Fab, Nanoprobed) in PBS containing 5% BSA and 0.05% saponin for 1 hour at room temperature.

5. The samples were fixed with 2% glutaraldehyde in PBS for 30 minutes at room temperature.

6. Silver enhancement of the samples was conducted using the HQ kit from Nanoprobes.

7. The samples were washed twice with deionized water, postfixed with 1% osmium tetroxide, dehydrated using increasing concentrations of ethanol, and embedded in 100% epoxy resin.

8. Ultrathin sections (70 nm thickness) were cut and stained with 1% uranyl acetate for 15 minutes and 3% lead citrate for 5 minutes.

9. Sections were examined using a Philips CM 100 Transmission Electron Microscope at 80 KV, and images were captured using the Gatan Orius CCD camera.

4-15 Immunofluorescence Stain

For immunofluorescence staining, the following steps were performed:

1. The cultured cells on cover slips were fixed with a 10% formaldehyde solution (HT501128, Sigma) for 10 minutes at room temperature.
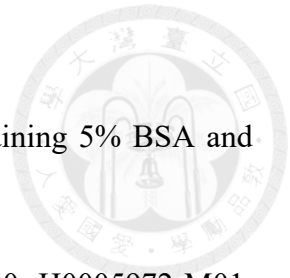
2. The fixed cells were washed three times with PBS for 5 minutes each.

3. Permeabilization of the cells was done using 0.1% Triton X-100 (108603,

Merck) for 10 minutes at room temperature, followed by another three washes

with PBS for 5 minutes each.

4. The cells were blocked in PBS containing 1% BSA for 30 minutes.

5. Primary antibodies were incubated with the cells overnight at 4°C in the

blocking buffer. The primary antibodies used were: mouse anti-renin (dilution:

1:50, H00005972-M01, Abnova); rabbit anti-calnexin (ab22595, Abcam); rabbit

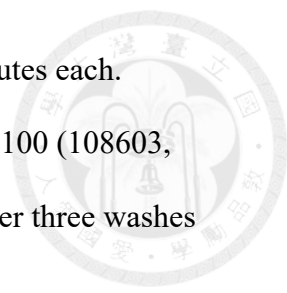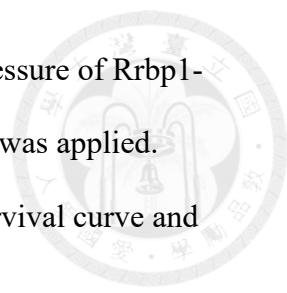anti-GOLIM4 (PAB28477, Abnova); rabbit anti-TGN46 (NBP1-49643,

NovusBio).

6. After incubation with the primary antibodies, the cells were washed three times

with PBS for 5 minutes each.

7. Secondary antibodies were applied to the cells for 1.5 hours at room

temperature. The secondary antibodies used were: Alexa Fluor® 488 goat anti-

mouse IgG(H+L) (dilution: 1:100, A11029, Thermo Fisher) or Alexa FluorTM

555 goat anti-rabbit IgG(H+L) (dilution: 1:100, A21428, Thermo Fisher).

8. Slides were mounted with a drop of DAPI Fluoromount-G® (0100-20,

Southern Biotech) for nuclear staining.

9. Samples were examined using a laser scanning confocal microscope Zeiss LSM

700. Confocal images were acquired with a 63× oil objective lens in a 1024 ×

1024 pixels format at a 12-bit intensity resolution.

4-16 Statistics

Statistical analyses were performed using the following methods:

1. Mean ± standard error of the mean (SEM) was used to represent all data.

2. For data sets comparing three independent groups (blood pressure of Rrbp1-WT, HE, and knockout mice), ordinary one-way ANOVA test was applied.

3. Survival analysis was conducted using the Kaplan-Meier survival curve and log-rank test.

4. For data sets that followed a normal distribution, unpaired, two-tailed Student's t-test ($p \leq 0.05$) was used for comparisons.

5. For data sets that did not follow a normal distribution, nonparametric tests, specifically the two-tailed Mann-Whitney U test ($p \leq 0.05$), were used for comparisons.

6. Representative images were selected from one of the repeat experiments that best matched the average data in each assay.
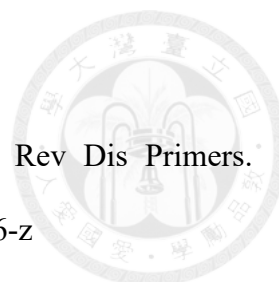
5. References

1. Libby P, Buring JE, Badimon L, et al. Atherosclerosis. Nat Rev Dis Primers. 2019;5(1):56. Published 2019 Aug 16. doi:10.1038/s41572-019-0106-z

2. Matsunaga H, Ito K, Akiyama M, et al. Transethnic Meta-Analysis of Genome-Wide Association Studies Identifies Three New Loci and Characterizes Population-Specific Differences for Coronary Artery Disease. Circ Genom Precis Med. 2020;13(3):e002670. doi:10.1161/CIRCGEN.119.002670

3. McPherson R, Pertsemlidis A, Kavaslar N, et al. A common allele on chromosome 9 associated with coronary heart disease. Science. 2007;316(5830):1488-1491. doi:10.1126/science.1142447

4. Samani NJ, Erdmann J, Hall AS, et al. Genome wide association analysis of coronary artery disease. N Engl J Med. 2007;357(5):443-453. doi:10.1056/NEJMoa072366

5. Wellcome Trust Case Control Consortium. Genome-wide association study of 14,000 cases of seven common diseases and 3,000 shared controls. Nature. 2007;447(7145):661-678. doi:10.1038/nature05911

6. Coronary Artery Disease Consortium, Samani NJ, Deloukas P, et al. Large scale association analysis of novel genetic loci for coronary artery disease. Arterioscler Thromb Vasc Biol. 2009;29(5):774-780. doi:10.1161/ATVBAHA.108.181388

7. Erdmann J, Grosshennig A, Braund PS, et al. New susceptibility locus for coronary artery disease on chromosome 3q22.3. Nat Genet. 2009;41(3):280-282. doi:10.1038/ng.307

8. Nikpay M, Goel A, Won HH, et al. A comprehensive 1,000 Genomes-based genome-wide association meta-analysis of coronary artery disease. Nat Genet. 2015;47(10):1121-1130. doi:10.1038/ng.3396

9. Helgadottir A, Thorleifsson G, Manolescu A, et al. A common variant on chromosome

9p21 affects the risk of myocardial infarction. Science. 2007;316(5830):1491-1493. doi:10.1126/science.1142842

10. Trégouët DA, König IR, Erdmann J, et al. Genome-wide haplotype association study identifies the SLC22A3-LPAL2-LPA gene cluster as a risk locus for coronary artery disease. Nat Genet. 2009;41(3):283-285. doi:10.1038/ng.314
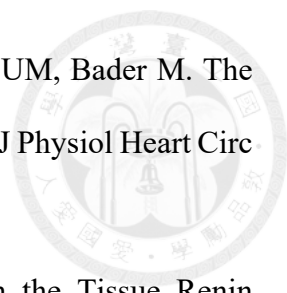
11. GBD 2017 Risk Factor Collaborators. Global, regional, and national comparative risk assessment of 84 behavioural, environmental and occupational, and metabolic risks or clusters of risks for 195 countries and territories, 1990-2017: a systematic analysis for the Global Burden of Disease Study 2017 [published correction appears in Lancet. 2019 Jan 12;393(10167):132] [published correction appears in Lancet. 2019 Jun 22;393(10190):e44].Lancet.2018;392(10159):1923-1994.doi:10.1016/S0140-6736(18)32225-6

12. Mills KT, Bundy JD, Kelly TN, et al. Global Disparities of Hypertension Prevalence and Control: A Systematic Analysis of Population-Based Studies From 90 Countries. Circulation. 2016;134(6):441-450. doi:10.1161/CIRCULATIONAHA.115.018912

13. GBD 2013 Risk Factors Collaborators, Forouzanfar MH, Alexander L, et al. Global, regional, and national comparative risk assessment of 79 behavioural, environmental and occupational, and metabolic risks or clusters of risks in 188 countries, 1990-2013: a systematic analysis for the Global Burden of Disease Study 2013. Lancet. 2015;386(10010):2287-2323. doi:10.1016/S0140-6736(15)00128-2

14. Ibrahim MM, Damasceno A. Hypertension in developing countries. Lancet. 2012;380(9841):611-619. doi:10.1016/S0140-6736(12)60861-7

15. Liu J, Zhou Y, Liu Y, et al. (Pro)renin receptor regulates lung development via the Wnt/β-catenin signaling pathway. Am J Physiol Lung Cell Mol Physiol. 2019;317(2):L202-L211. doi:10.1152/ajplung.00295.2018

16. Santos RAS, Oudit GY, Verano-Braga T, Canta G, Steckelings UM, Bader M. The renin-angiotensin system: going beyond the classical paradigms. Am J Physiol Heart Circ Physiol. 2019;316(5):H958-H970. doi:10.1152/ajpheart.00723.2018

17. Nehme A, Zouein FA, Zayeri ZD, Zibara K. An Update on the Tissue Renin Angiotensin System and Its Role in Physiology and Pathology. J Cardiovasc Dev Dis. 2019;6(2):14. Published 2019 Mar 29. doi:10.3390/jcdd6020014

18. Sinn PL, Zhang X, Sigmund CD. JG cell expression and partial regulation of a human renin genomic transgene driven by a minimal renin promoter. Am J Physiol. 1999;277(4):F634-F642. doi:10.1152/ajprenal.1999.277.4.F634

19. Fountain JH, Lappin SL. Physiology, Renin Angiotensin System. In: StatPearls. Treasure Island (FL): StatPearls Publishing; June 18, 2022.

20. Wu C, Lu H, Cassis LA, Daugherty A. Molecular and Pathophysiological Features of Angiotensinogen: A Mini Review. N Am J Med Sci (Boston). 2011;4(4):183-190. doi:10.7156/v4i4p183

21. Lu H, Cassis LA, Kooi CW, Daugherty A. Structure and functions of angiotensinogen [published correction appears in Hypertens Res. 2016 Nov;39(11):827]. Hypertens Res. 2016;39(7):492-500. doi:10.1038/hr.2016.17

22. Fukamizu A, Sugimura K, Takimoto E, et al. Chimeric renin-angiotensin system demonstrates sustained increase in blood pressure of transgenic mice carrying both human renin and human angiotensinogen genes. J Biol Chem. 1993;268(16):11617-11621.

23. Hatae T, Takimoto E, Murakami K, Fukamizu A. Comparative studies on species-specific reactivity between renin and angiotensinogen. Mol Cell Biochem. 1994;131(1):43-47. doi:10.1007/BF01075723

24. HELMER OM. Differentiation between two forms of angiotonin by means of spirally

cut strips of rabbit aorta. Am J Physiol. 1957;188(3):571-577. doi:10.1152/ajplegacy.1957.188.3.571

25. Yang HY, Erdös EG, Levin Y. A dipeptidyl carboxypeptidase that converts angiotensin I and inactivates bradykinin. Biochim Biophys Acta. 1970;214(2):374-376. doi:10.1016/0005-2795(70)90017-6

26. Erdös EG. Conversion of angiotensin I to angiotensin II. Am J Med. 1976;60(6):749-759. doi:10.1016/0002-9343(76)90889-5

27. Skidgel RA, Erdös EG. Angiotensin converting enzyme (ACE) and neprilysin hydrolyze neuropeptides: a brief history, the beginning and follow-ups to early studies. Peptides. 2004;25(3):521-525. doi:10.1016/j.peptides.2003.12.010

28. Yoshida T, Nosaka S. Some characteristics of a peptidyl dipeptidase (kininase II) from rat CSF: differential effects of NaCl on the sequential degradation steps of bradykinin. J Neurochem. 1990;55(6):1861-1869. doi:10.1111/j.1471-4159.1990.tb05769.x

29. Abadir PM, Foster DB, Crow M, et al. Identification and characterization of a functional mitochondrial angiotensin system. Proc Natl Acad Sci U S A. 2011;108(36):14849-14854. doi:10.1073/pnas.1101507108

30. Adiarto S, Heiden S, Vignon-Zellweger N, et al. ET-1 from endothelial cells is required for complete angiotensin II-induced cardiac fibrosis and hypertrophy. Life Sci. 2012;91(13-14):651-657. doi:10.1016/j.lfs.2012.02.006

31. Barhoumi T, Kasal DA, Li MW, et al. T regulatory lymphocytes prevent angiotensin II-induced hypertension and vascular injury. Hypertension. 2011;57(3):469-476. doi:10.1161/HYPERTENSIONAHA.110.162941

32. Bendall JK, Cave AC, Heymes C, Gall N, Shah AM. Pivotal role of a gp91(phox)-containing NADPH oxidase in angiotensin II-induced cardiac hypertrophy in mice.

Circulation. 2002;105(3):293-296. doi:10.1161/hc0302.103712

33. Santos RAS, Sampaio WO, Alzamora AC, et al. The ACE2/Angiotensin-(1-7)/MAS Axis of the Renin-Angiotensin System: Focus on Angiotensin-(1-7). Physiol Rev. 2018;98(1):505-553. doi:10.1152/physrev.00023.2016

34. Falkenstein E, Tillmann HC, Christ M, Feuring M, Wehling M. Multiple actions of steroid hormones--a focus on rapid, nongenomic effects. Pharmacol Rev. 2000;52(4):513-556.

35. Harvey BJ, Condliffe S, Doolan CM. Sex and salt hormones: rapid effects in epithelia. News Physiol Sci. 2001;16:174-177. doi:10.1152/physiologyonline.2001.16.4.174

36. Náray-Fejes-Tóth A, Fejes-Tóth G. The sgk, an aldosterone-induced gene in mineralocorticoid target cells, regulates the epithelial sodium channel. Kidney Int. 2000;57(4):1290-1294. doi:10.1046/j.1523-1755.2000.00964.x

37. Verrey F. Early aldosterone action: toward filling the gap between transcription and transport. Am J Physiol. 1999;277(3):F319-F327. doi:10.1152/ajprenal.1999.277.3.F319
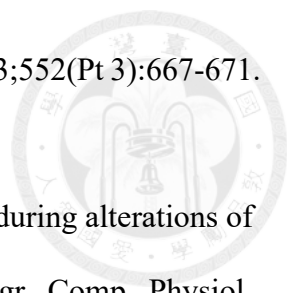
38. Booth RE, Johnson JP, Stockand JD. Aldosterone. Adv Physiol Educ. 2002;26(1-4):8-20. doi:10.1152/advan.00051.2001

39. Kim GH, Masilamani S, Turner R, Mitchell C, Wade JB, Knepper MA. The thiazide-sensitive Na-Cl cotransporter is an aldosterone-induced protein. Proc Natl Acad Sci U S A. 1998;95(24):14552-14557. doi:10.1073/pnas.95.24.14552

40. Cho JH, Musch MW, Bookstein CM, McSwine RL, Rabenau K, Chang EB. Aldosterone stimulates intestinal Na+ absorption in rats by increasing NHE3 expression of the proximal colon. Am J Physiol. 1998;274(3):C586-C594. doi:10.1152/ajpcell.1998.274.3.C586

41. Kurtz A. Control of renin synthesis and secretion. Am J Hypertens. 2012;25(8):839-847. doi:10.1038/ajh.2011.246
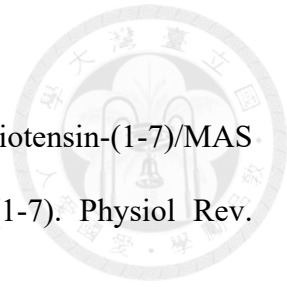
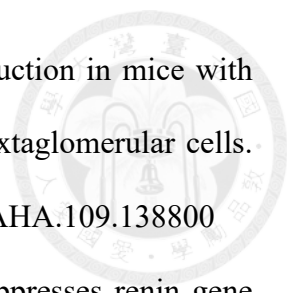42. Persson PB. Renin: origin, secretion and synthesis. J Physiol. 2003;552(Pt 3):667-671. doi:10.1113/jphysiol.2003.049890

43. Cholewa BC, Mattson DL. Role of the renin-angiotensin system during alterations of sodium intake in conscious mice. Am J Physiol Regul Integr Comp Physiol. 2001;281(3):R987-R993. doi:10.1152/ajpregu.2001.281.3.R987

44. Peters J, Clausmeyer S. Intracellular sorting of renin: cell type specific differences and their consequences. J Mol Cell Cardiol. 2002;34(12):1561-1568. doi:10.1006/jmcc.2002.2079

45. Clausmeyer S, Stürzebecher R, Peters J. An alternative transcript of the rat renin gene can result in a truncated prorenin that is transported into adrenal mitochondria. Circ Res. 1999;84(3):337-344. doi:10.1161/01.res.84.3.337

46. Wanka H, Kessler N, Ellmer J, et al. Cytosolic renin is targeted to mitochondria and induces apoptosis in H9c2 rat cardiomyoblasts. J Cell Mol Med. 2009;13(9A):2926-2937. doi:10.1111/j.1582-4934.2008.00448.x

47. Peters J, Wanka H, Peters B, Hoffmann S. A renin transcript lacking exon 1 encodes for a non-secretory intracellular renin that increases aldosterone production in transgenic rats. J Cell Mol Med. 2008;12(4):1229-1237. doi:10.1111/j.1582-4934.2008.00132.x

48. De Mello WC, Frohlich ED. On the local cardiac renin angiotensin system. Basic and clinical implications. Peptides. 2011;32(8):1774-1779. doi:10.1016/j.peptides.2011.06.018

49. Pan L, Gross KW. Transcriptional regulation of renin: an update. Hypertension. 2005;45(1):3-8. doi:10.1161/01.HYP.0000149717.55920.45

50. Gomez RA, Pentz ES, Jin X, Cordaillat M, Sequeira Lopez ML. CBP and p300 are essential for renin cell identity and morphological integrity of the kidney. Am J Physiol Heart Circ Physiol. 2009;296(5):H1255-H1262. doi:10.1152/ajpheart.01266.2008

51. Desch M, Schreiber A, Schweda F, et al. Increased renin production in mice with deletion of peroxisome proliferator-activated receptor-gamma in juxtaglomerular cells. Hypertension. 2010;55(3):660-666. doi:10.1161/HYPERTENSIONAHA.109.138800

52. Yuan W, Pan W, Kong J, et al. 1,25-dihydroxyvitamin D3 suppresses renin gene transcription by blocking the activity of the cyclic AMP response element in the renin gene promoter. J Biol Chem. 2007;282(41):29821-29830. doi:10.1074/jbc.M705495200

53. Todorov VT, Völkl S, Müller M, et al. Tumor necrosis factor-alpha activates NFkappaB to inhibit renin transcription by targeting cAMP-responsive element. J Biol Chem. 2004;279(2):1458-1467. doi:10.1074/jbc.M308697200

54. Pratt RE, Carleton JE, Richie JP, Heusser C, Dzau VJ. Human renin biosynthesis and secretion in normal and ischemic kidneys. Proc Natl Acad Sci U S A. 1987;84(22):7837-7840. doi:10.1073/pnas.84.22.7837

55. Danser AH, Deinum J. Renin, prorenin and the putative (pro)renin receptor. Hypertension. 2005;46(5):1069-1076. doi:10.1161/01.HYP.0000186329.92187.2e

56. Nguyen G, Muller DN. The biology of the (pro)renin receptor. J Am Soc Nephrol. 2010;21(1):18-23. doi:10.1681/ASN.2009030300

57. Brakch N, Allemandou F, Keller I, Nussberger J. The renin prosequence enhances constitutive secretion of renin and optimizes renin activity. Curr Neurovasc Res. 2011;8(2):121-130. doi:10.2174/156720211795495367

58. Sequeira Lopez ML, Gomez RA. Novel mechanisms for the control of renin synthesis and release. Curr Hypertens Rep. 2010;12(1):26-32. doi:10.1007/s11906-009-0080-z

59. Torretti J. Sympathetic control of renin release. Annu Rev Pharmacol Toxicol. 1982;22:167-192. doi:10.1146/annurev.pa.22.040182.001123

60. Persson AE, Ollerstam A, Liu R, Brown R. Mechanisms for macula densa cell release of renin. Acta Physiol Scand. 2004;181(4):471-474. doi:10.1111/j.1365-

201X.2004.01320.x

61. Watanabe H, Belyea BC, Paxton RL, et al. Renin Cell Baroreceptor, a Nuclear Mechanotransducer Central for Homeostasis. Circ Res. 2021;129(2):262-276. doi:10.1161/CIRCRESAHA.120.318711

62. Feldman RD, Gros R. New insights into the regulation of cAMP synthesis beyond GPCR/G protein activation: implications in cardiovascular regulation. Life Sci. 2007;81(4):267-271. doi:10.1016/j.lfs.2007.05.015

63. Beierwaltes WH. The role of calcium in the regulation of renin secretion. Am J Physiol Renal Physiol. 2010;298(1):F1-F11. doi:10.1152/ajprenal.00143.2009

64. Sousa AG, Cabral JV, El-Feghaly WB, de Sousa LS, Nunes AB. Hyporeninemic hypoaldosteronism and diabetes mellitus: Pathophysiology assumptions, clinical aspects and implications for management. World J Diabetes. 2016;7(5):101-111. doi:10.4239/wjd.v7.i5.101

65. Chelaghma N, Oyibo SO. Hyporeninemic hypoaldosteronism in a patient with diabetes mellitus: an unforgettable case report. Int Med Case Rep J. 2018;11:69-72. Published 2018 Apr 3. doi:10.2147/IMCRJ.S158628
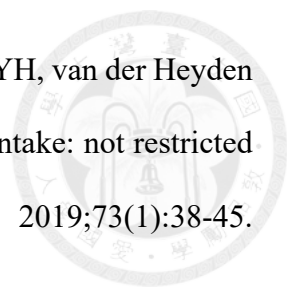
66. Grande Villoria J, Macias Nunez JF, Miralles JM, De Castro del Pozo S, Tabernero Romo JM. Hyporeninemic hypoaldosteronism in diabetic patients with chronic renal failure. Am J Nephrol. 1988;8(2):127-137. doi:10.1159/000167571

67. DeFronzo RA. Hyperkalemia and hyporeninemic hypoaldosteronism. Kidney Int. 1980;17(1):118-134. doi:10.1038/ki.1980.14

68. Tan SY, Burton M. Hyporeninemic hypoaldosteronism. An overlooked cause of hyperkalemia. Arch Intern Med. 1981;141(1):30-33. doi:10.1001/archinte.141.1.30

69. Hollander-Rodriguez JC, Calvert JF Jr. Hyperkalemia. Am Fam Physician. 2006;73(2):283-290.
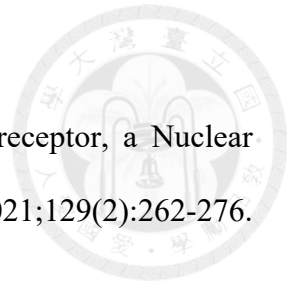
70. Te Dorsthorst RPM, Hendrikse J, Vervoorn MT, van Weperen VYH, van der Heyden MAG. Review of case reports on hyperkalemia induced by dietary intake: not restricted to chronic kidney disease patients. Eur J Clin Nutr. 2019;73(1):38-45. doi:10.1038/s41430-018-0154-6

71. Palmer BF, Clegg DJ. Physiology and Pathophysiology of Potassium Homeostasis: Core Curriculum 2019. Am J Kidney Dis. 2019;74(5):682-695. doi:10.1053/j.ajkd.2019.03.427

72. Watanabe T, Nitta K. Transient hyporeninemic hypoaldosteronism in acute glomerulonephritis. Pediatr Nephrol. 2002;17(11):959-963. doi:10.1007/s00467-002-0984-1

73. Malik WA, Labib MH, Irfan H. Hyporeninaemic hypoaldosteronism and systemic amyloidosis. Ann Clin Biochem. 1995;32 (Pt 6):593-594. doi:10.1177/000456329503200614

74. Schnermann J. Juxtaglomerular cell complex in the regulation of renal salt excretion. Am J Physiol. 1998;274(2):R263-R279. doi:10.1152/ajpregu.1998.274.2.R263

75. Alhenc-Gelas F. A new channel for the control of renin secretion in juxtaglomerular cells. Kidney Int. 2020;98(3):543-545. doi:10.1016/j.kint.2020.05.031

76. Wanker EE, Sun Y, Savitz AJ, Meyer DI. Functional characterization of the 180-kD ribosome receptor in vivo. J Cell Biol. 1995;130(1):29-39. doi:10.1083/jcb.130.1.29

77. Benyamini P, Webster P, Meyer DI. KD of p180 eliminates the terminal differentiation of a secretory cell line. Mol Biol Cell. 2009;20(2):732-744. doi:10.1091/mbc.e08-07-0682

78. Savitz AJ, Meyer DI. 180-kD ribosome receptor is essential for both ribosome binding and protein translocation. J Cell Biol. 1993;120(4):853-863. doi:10.1083/jcb.120.4.853

79. Cui XA, Zhang H, Palazzo AF. p180 promotes the ribosome-independent localization

of a subset of mRNA to the endoplasmic reticulum. PLoS Biol. 2012;10(5):e1001336. doi:10.1371/journal.pbio.1001336

80. Ueno T, Kaneko K, Sata T, Hattori S, Ogawa-Goto K. Regulation of polysome assembly on the endoplasmic reticulum by a coiled-coil protein, p180. Nucleic Acids Res. 2012;40(7):3006-3017. doi:10.1093/nar/gkr1197

81. Ogawa-Goto K, Tanaka K, Ueno T, et al. p180 is involved in the interaction between the endoplasmic reticulum and microtubules through a novel microtubule-binding and bundling domain. Mol Biol Cell. 2007;18(10):3741-3751. doi:10.1091/mbc.e06-12-1125

82. Bai JZ, Leung E, Holloway H, Krissansen GW. Alternatively spliced forms of the P180 ribosome receptor differ in their ability to induce the proliferation of rough endoplasmic reticulum. Cell Biol Int. 2008;32(5):473-483. doi:10.1016/j.cellbi.2007.10.002

83. Becker F, Block-Alper L, Nakamura G, Harada J, Wittrup KD, Meyer DI. Expression of the 180-kD ribosome receptor induces membrane proliferation and increased secretory activity in yeast. J Cell Biol. 1999;146(2):273-284. doi:10.1083/jcb.146.2.273

84. Ueno T, Tanaka K, Kaneko K, et al. Enhancement of procollagen biosynthesis by p180 through augmented ribosome association on the endoplasmic reticulum in response to stimulated secretion. J Biol Chem. 2010;285(39):29941-29950. doi:10.1074/jbc.M109.094607

85. Yasuno K, Bakırcıoğlu M, Low SK, et al. Common variant near the endothelin receptor type A (EDNRA) gene is associated with intracranial aneurysm risk. Proc Natl Acad Sci U S A. 2011;108(49):19707-19712. doi:10.1073/pnas.1117137108

86. Vuckovic D, Bao EL, Akbari P, et al. The Polygenic and Monogenic Basis of Blood Traits and Diseases. Cell. 2020;182(5):1214-1231.e11. doi:10.1016/j.cell.2020.08.008

87. van der Harst P, Verweij N. Identification of 64 Novel Genetic Loci Provides an
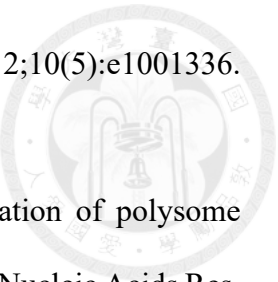
Expanded View on the Genetic Architecture of Coronary Artery Disease. Circ Res. 2018;122(3):433-443. doi:10.1161/CIRCRESAHA.117.312086

88. Anastasia I, Ilacqua N, Raimondi A, et al. Mitochondria-rough-ER contacts in the liver regulate systemic lipid homeostasis. Cell Rep. 2021;34(11):108873. doi:10.1016/j.celrep.2021.108873

89. Boini KM, Nammi S, Grahammer F, Osswald H, Kuhl D, Lang F. Role of serum- and glucocorticoid-inducible kinase SGK1 in glucocorticoid regulation of renal electrolyte excretion and blood pressure. Kidney Blood Press Res. 2008;31(4):280-289. doi:10.1159/000151666

90. Iravanian S, Dudley SC Jr. The renin-angiotensin-aldosterone system (RAAS) and cardiac arrhythmias [published correction appears in Heart Rhythm. 2008 Oct;5(10):1499]. Heart Rhythm. 2008;5(6 Suppl):S12-S17. doi:10.1016/j.hrthm.2008.02.025

91. Chuang LM, Chiu YF, Sheu WH, et al. Biethnic comparisons of autosomal genomic scan for loci linked to plasma adiponectin in populations of Chinese and Japanese origin. J Clin Endocrinol Metab. 2004;89(11):5772-5778. doi:10.1210/jc.2004-0640

92. Lange C, Silverman EK, Xu X, Weiss ST, Laird NM. A multivariate family-based association test using generalized estimating equations: FBAT-GEE. Biostatistics. 2003;4(2):195-206. doi:10.1093/biostatistics/4.2.195

93. Liu P, Jenkins NA, Copeland NG. A highly efficient recombineering-based method for generating conditional knockout mutations. Genome Res. 2003;13(3):476-484. doi:10.1101/gr.749203

94. Huang CH, Shih YY, Siow TY, et al. Temporal assessment of vascular reactivity and functionality using MRI during postischemic proangiogenenic vascular remodeling. Magn Reson Imaging. 2015;33(7):903-910. doi:10.1016/j.mri.2015.04.009
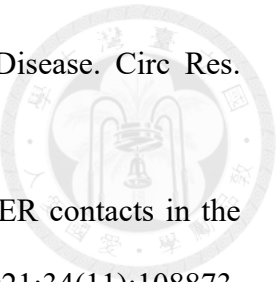
95. Hsiao HY, Chen YC, Huang CH, et al. Aberrant astrocytes impair vascular reactivity in Huntington disease. Ann Neurol. 2015;78(2):178-192. doi:10.1002/ana.24428

96. Cesarovic N, Jirkof P, Rettich A, Arras M. Implantation of radiotelemetry transmitters yielding data on ECG, heart rate, core body temperature and activity in free-moving laboratory mice. J Vis Exp. 2011;(57):3260. Published 2011 Nov 21. doi:10.3791/3260

97. Shendre A, Irvin MR, Wiener H, et al. Local Ancestry and Clinical Cardiovascular Events Among African Americans From the Atherosclerosis Risk in Communities Study. J Am Heart Assoc. 2017;6(4):e004739. Published 2017 Apr 10. doi:10.1161/JAHA.116.004739

98. Richardson TG, Sanderson E, Palmer TM, et al. Evaluating the relationship between circulating lipoprotein lipids and apolipoproteins with risk of coronary heart disease: A multivariable Mendelian randomisation analysis. PLoS Med. 2020;17(3):e1003062. Published 2020 Mar 23. doi:10.1371/journal.pmed.1003062

99. Backman JD, Li AH, Marcketta A, et al. Exome sequencing and analysis of 454,787 UK Biobank participants. Nature. 2021;599(7886):628-634. doi:10.1038/s41586-021-04103-z

100. Paquette M, Chong M, Thériault S, Dufour R, Paré G, Baass A. Polygenic risk score predicts prevalence of cardiovascular disease in patients with familial hypercholesterolemia. J Clin Lipidol. 2017;11(3):725-732.e5. doi:10.1016/j.jacl.2017.03.019

101. Huikuri HV, Castellanos A, Myerburg RJ. Sudden death due to cardiac arrhythmias. N Engl J Med. 2001;345(20):1473-1482. doi:10.1056/NEJMra000650

102. Weiner ID, Wingo CS. Hyperkalemia: a potential silent killer. J Am Soc Nephrol. 1998;9(8):1535-1543. doi:10.1681/ASN.V981535

103. Webster A, Brady W, Morris F. Recognising signs of danger: ECG changes resulting

from an abnormal serum potassium concentration. Emerg Med J. 2002;19(1):74-77. doi:10.1136/emj.19.1.74

104. Mattu A, Brady WJ, Robinson DA. Electrocardiographic manifestations of hyperkalemia. Am J Emerg Med. 2000;18(6):721-729. doi:10.1053/ajem.2000.7344

105. Littmann L, Gibbs MA. Electrocardiographic manifestations of severe hyperkalemia. J Electrocardiol. 2018;51(5):814-817. doi:10.1016/j.jelectrocard.2018.06.018

106. Rastegar A, Soleimani M. Hypokalaemia and hyperkalaemia [published correction appears in Postgrad Med J 2002 Feb;78(916):126. Rastergar A [corrected to Rastegar A]]. Postgrad Med J. 2001;77(914):759-764. doi:10.1136/pmj.77.914.759

107. Shinagawa T, Do YS, Baxter J, Hsueh WA. Purification and characterization of human truncated prorenin. Biochemistry. 1992;31(10):2758-2764. doi:10.1021/bi00125a016

108. Hirose S, Kim S, Miyazaki H, Park YS, Murakami K. In vitro biosynthesis of human renin and identification of plasma inactive renin as an activation intermediate. J Biol Chem. 1985;260(30):16400-16405.

109. Lang JA, Yang G, Kern JA, Sigmund CD. Endogenous human renin expression and promoter activity in CALU-6, a pulmonary carcinoma cell line. Hypertension. 1995;25(4 Pt 2):704-710. doi:10.1161/01.hyp.25.4.704

110. Schambelan M, Sebastian A, Biglieri EG. Prevalence, pathogenesis, and functional significance of aldosterone deficiency in hyperkalemic patients with chronic renal insufficiency. Kidney Int. 1980;17(1):89-101. doi:10.1038/ki.1980.11

111. deLeiva A, Christlieb AR, Melby JC, et al. Big renin and biosynthetic defect of aldosterone in diabetes mellitus. N Engl J Med. 1976;295(12):639-643. doi:10.1056/NEJM197609162951203

112. Ranade K, Wu KD, Risch N, et al. Genetic variation in aldosterone synthase predicts
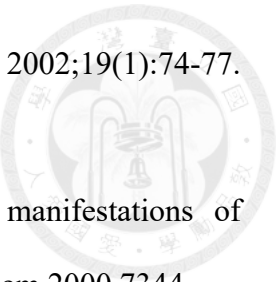
plasma glucose levels. Proc Natl Acad Sci U S A. 2001;98(23):13219-13224. doi:10.1073/pnas.221467098

113. Chiu CH, Hsuan CF, Lin SH, et al. ER ribosomal-binding protein 1 regulates blood pressure and potassium homeostasis by modulating intracellular renin trafficking. J Biomed Sci. 2023;30(1):13. Published 2023 Feb 19. doi:10.1186/s12929-023-00905-7